Astroparticle Physics 2022/23

1. Historical introduction - basic properties of cosmic rays
2. Hadronic interactions and accelerator data
3. Cascade equations
4. Electromagnetic cascades
5. Extensive air showers
6. Detectors for extensive air showers
7. High-energy cosmic rays and the knee in the energy spectrum of cosmic rays
8. Radio detection of extensive air showers
9. Acceleration, Astrophysical accelerators and beam dumps
10. Extragalactic propagation of cosmic rays
11. Ultra-high-energy energy cosmic rays
12. Astrophysical gamma rays and neutrinos
13. Neutrino astronomy
14. Gamma-ray astronomy

lecture 6
Detectors for extensive air showers

Gaisser chapter 16

16 Extensive air showers

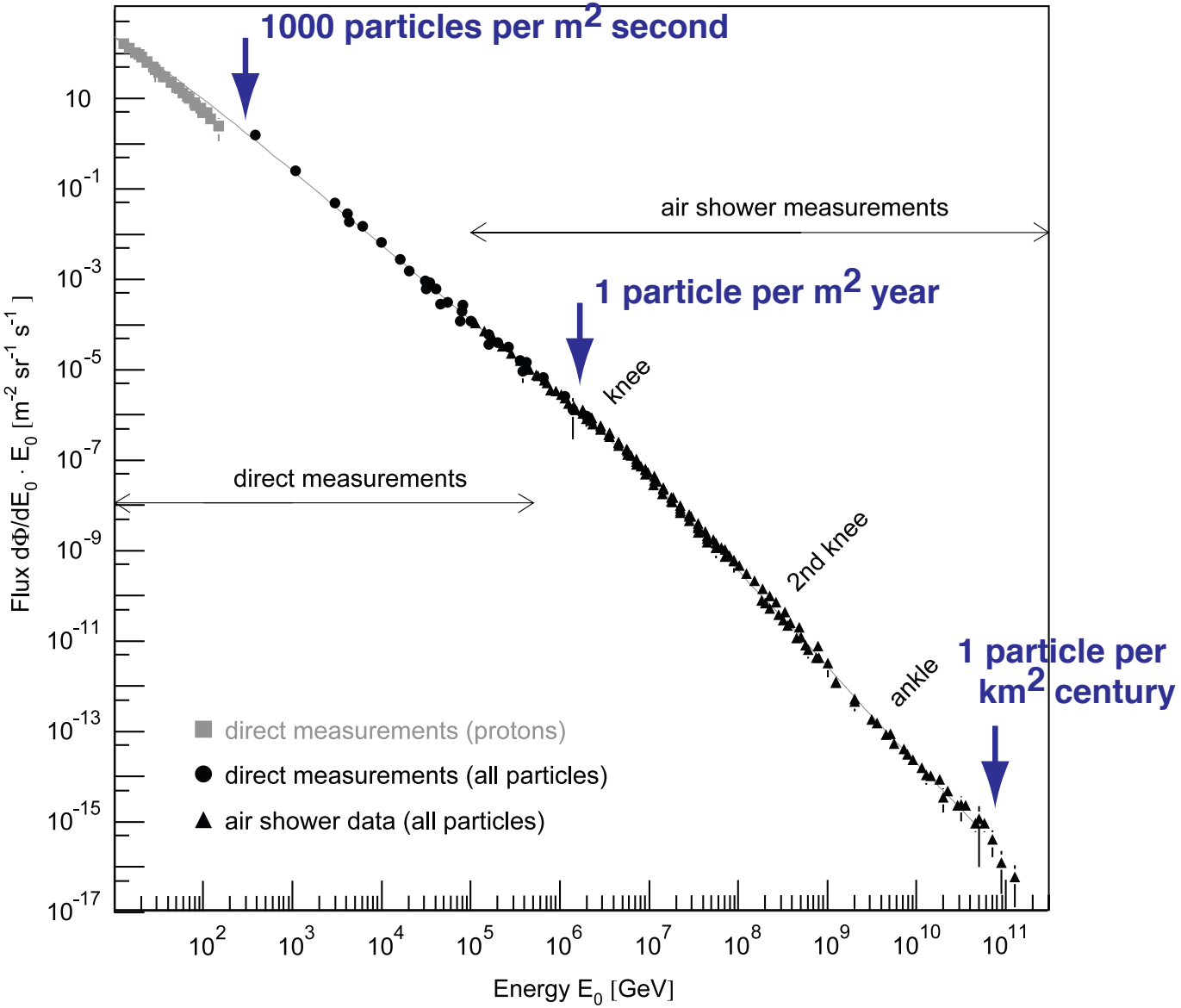

Fig. 1. All-particle energy spectrum of cosmic rays as measured directly with detectors above the atmosphere and with air shower detectors. At low energies, the flux of primary protons is shown.

Measurement of Cosmic Rays at E>10 TeV

Extensive Air Showers

flux falls ~$E^{-2.7}$ --> E=10^{15} eV: 1 particle/m²/a

atmosphere acts as an absorber/calorimeter

vertical atmospheric depth

$$1035 \ \frac{\mathrm{g}}{\mathrm{cm}^2}$$

$$\approx 12\lambda_I$$

$$\approx 30 X_0$$

--> calorimetric measurement

Extensive Air Shower

Proton 10^{15} eV:
on ground
10^6 particles
80% photons
18% electr./positr.
1.7% muons
0.3% hadrons

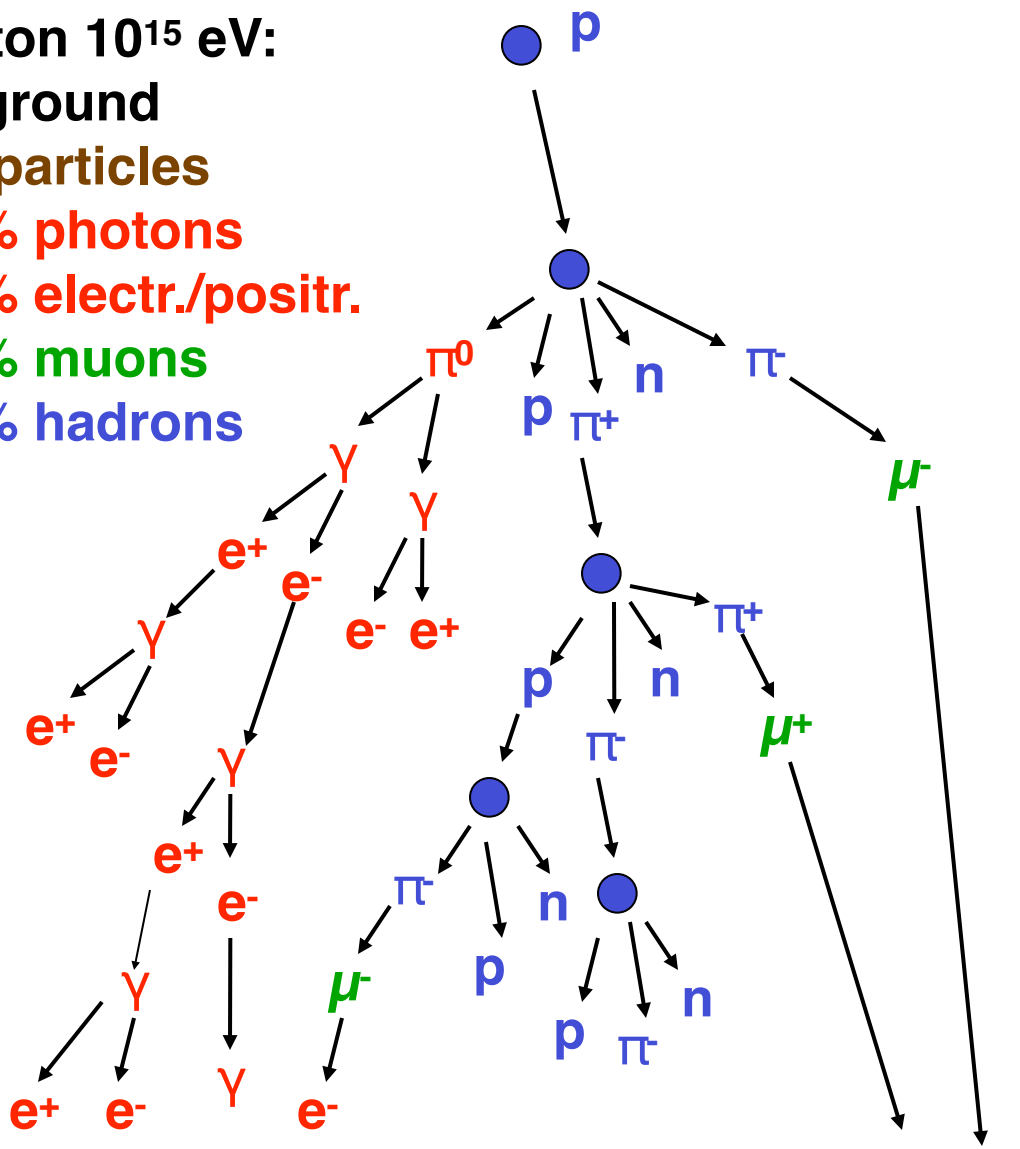

electromagnetic **hadronic** **muonic**

shower component

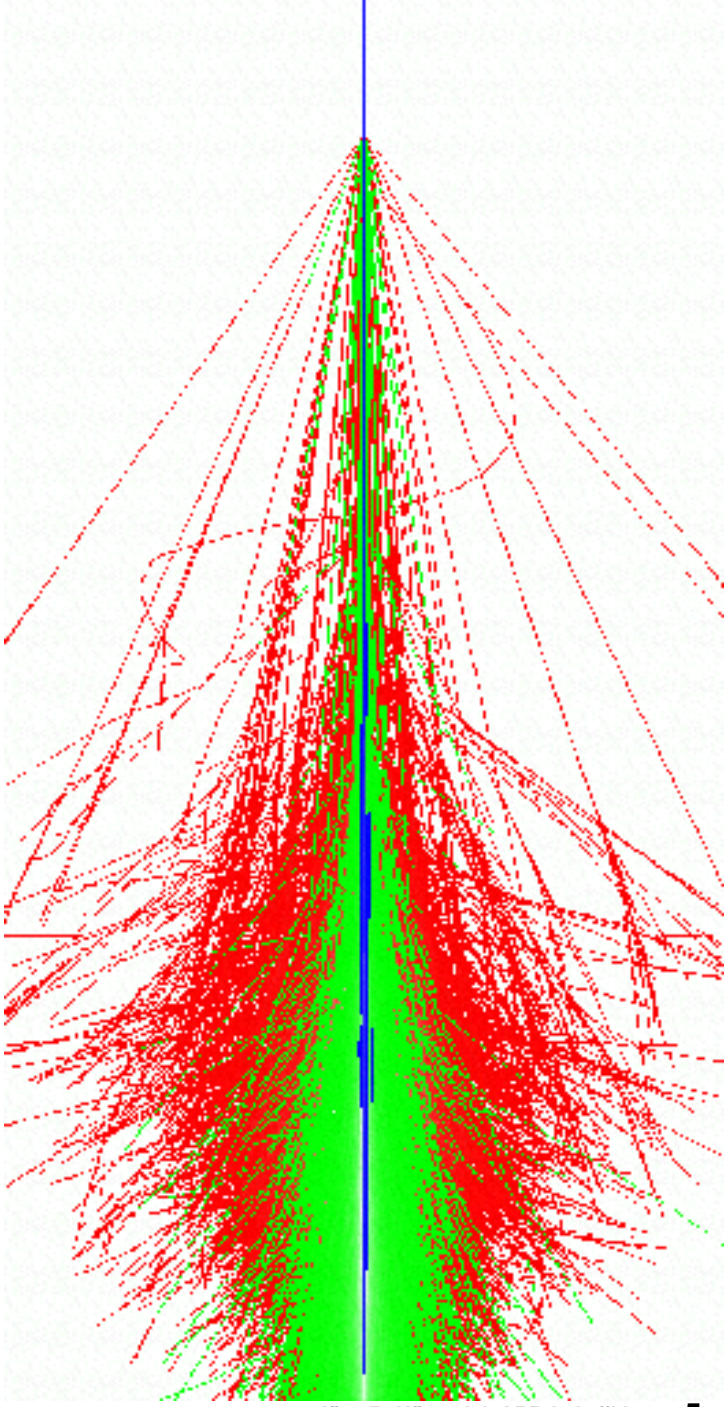

examples of showers with same (total) energy

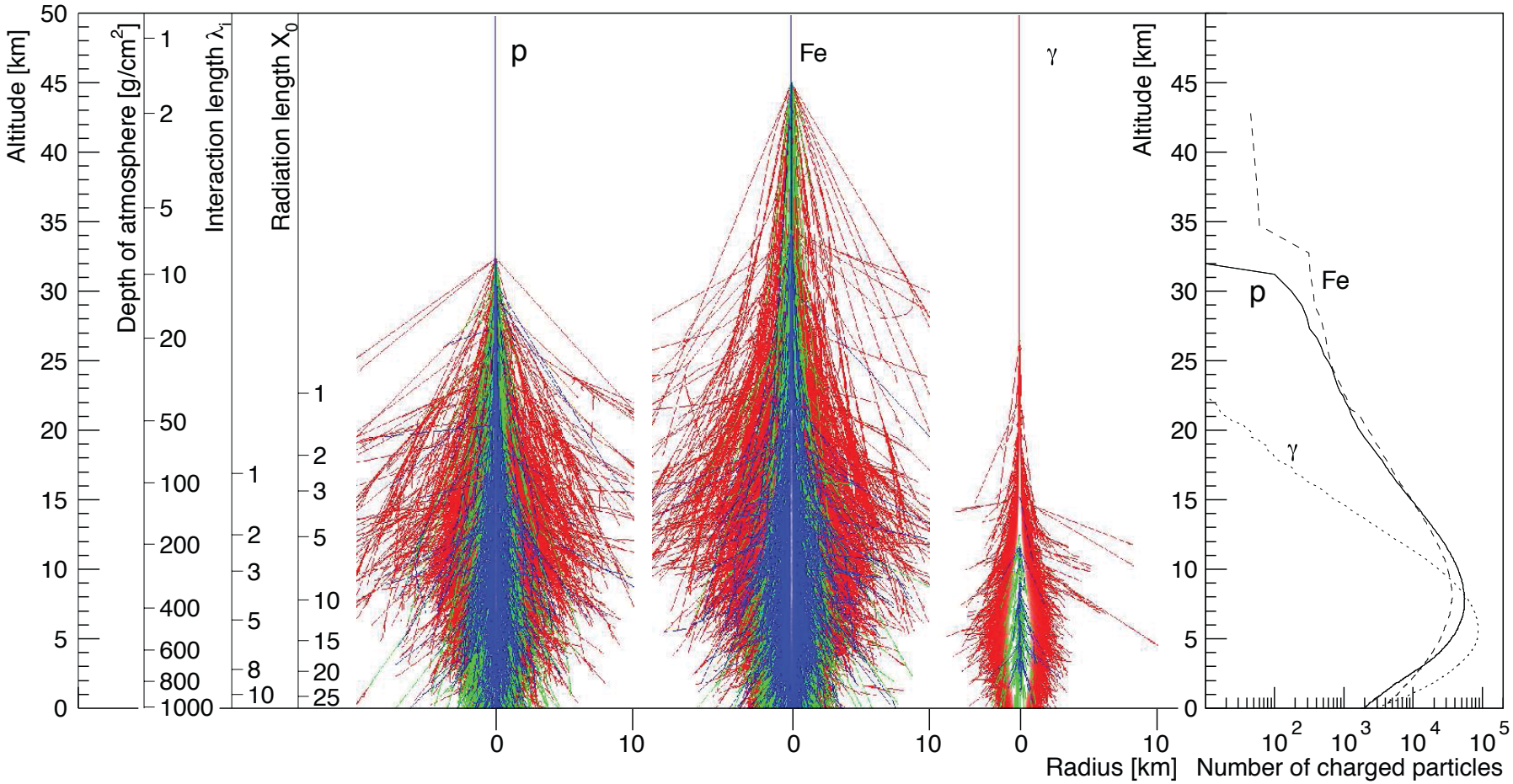

16.7 Particle detector arrays

Surface detector arrays consist of a set of particle detectors that are typically arranged in a regular pattern. Depending on the energy range the experiment is optimized for, the distance between the detector stations can vary from ~15 m (KASCADE [536], Tibet AS-γ [537]) up to more than 1000 m (Telescope Array [30], Auger Observatory [29]).

Showers are detected by searching for time coincidences of signals in neighboring detector stations. The arrival direction can then be determined from the time delay of the shower front reaching the different detectors. The shower comprises a disk of particles that is a few meters thick in the center, increasing up to a few hundred meters at large lateral distances. Only at small lateral distances can the curvature of the shower front be approximated as a sphere. The angular resolution of the reconstructed arrival direction depends on the distance and accuracy of time synchronization between the detector stations and the number of particles detected per station (for defining the arrival time of the shower front). Air shower arrays reach angular resolutions of typically $1 - 2^\circ$ for low-energy showers and better than 0.5° for large showers.

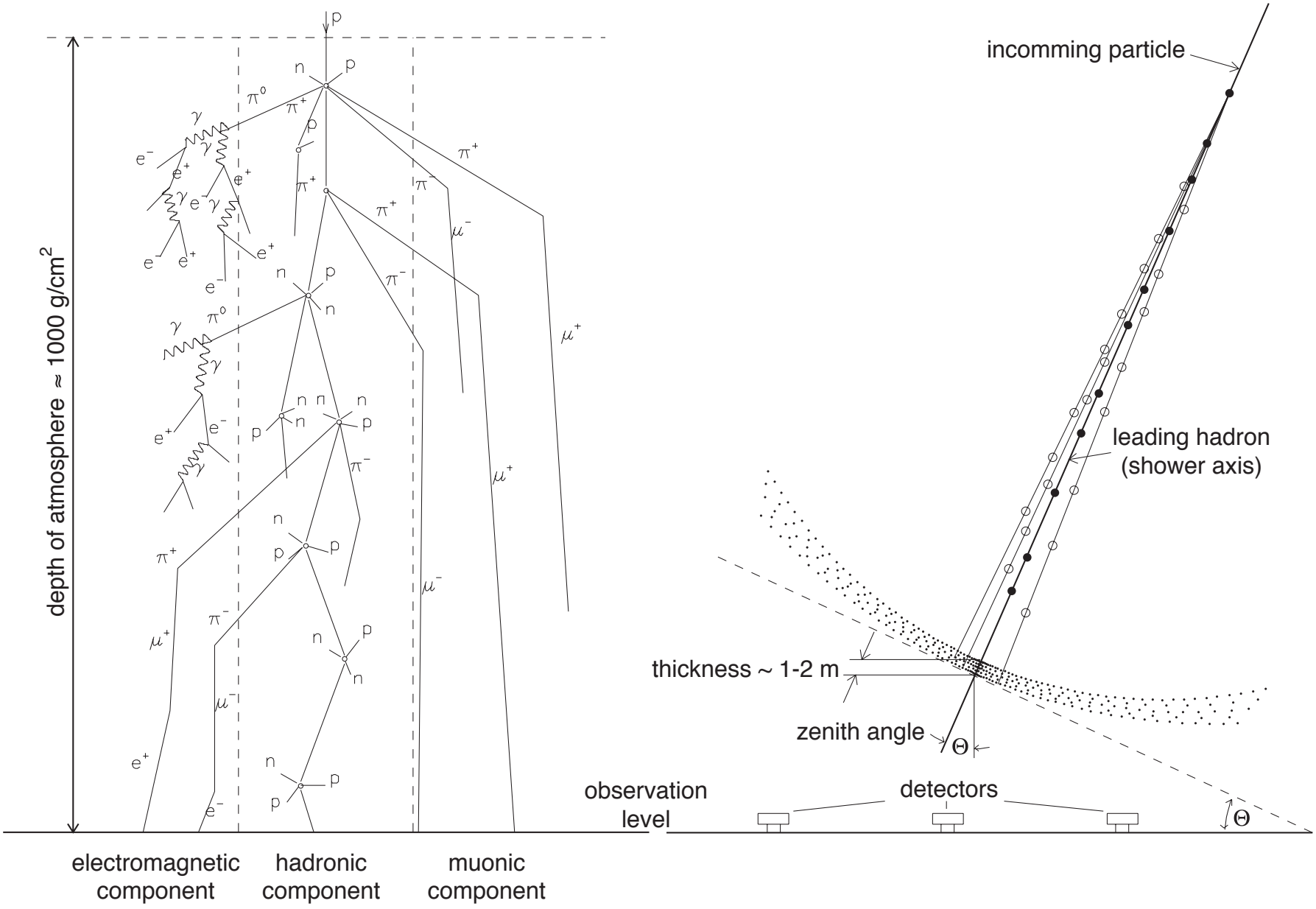
depth of atmosphere ≈ 1000 g/cm²
incomming particle
leading hadron
(shower axis)
thickness ~ 1-2 m
zenith angle
Θ
observation
level
detectors
Θ
electromagnetic
component
hadronic
component
muonic
component

Measurement methods

particles at ground

cascade of secondary particles allows to sample the shower at specific points

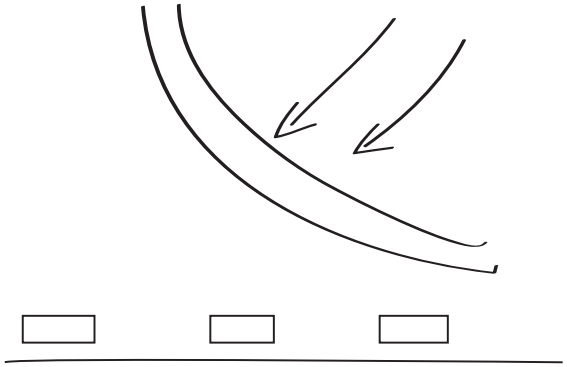

detector coverage
10^{15} eV: 1% (15 m)
10^{20} eV: 10^{-8} (1.5 km)

example: KASCADE 40000 m² total area
500 m² e/m detectors (~1.2%), detector distance 13 m

KArlsruhe Shower Core and Array DEtector

Simultaneous measurement of
electromagnetic,
muonic,
hadronic
shower components

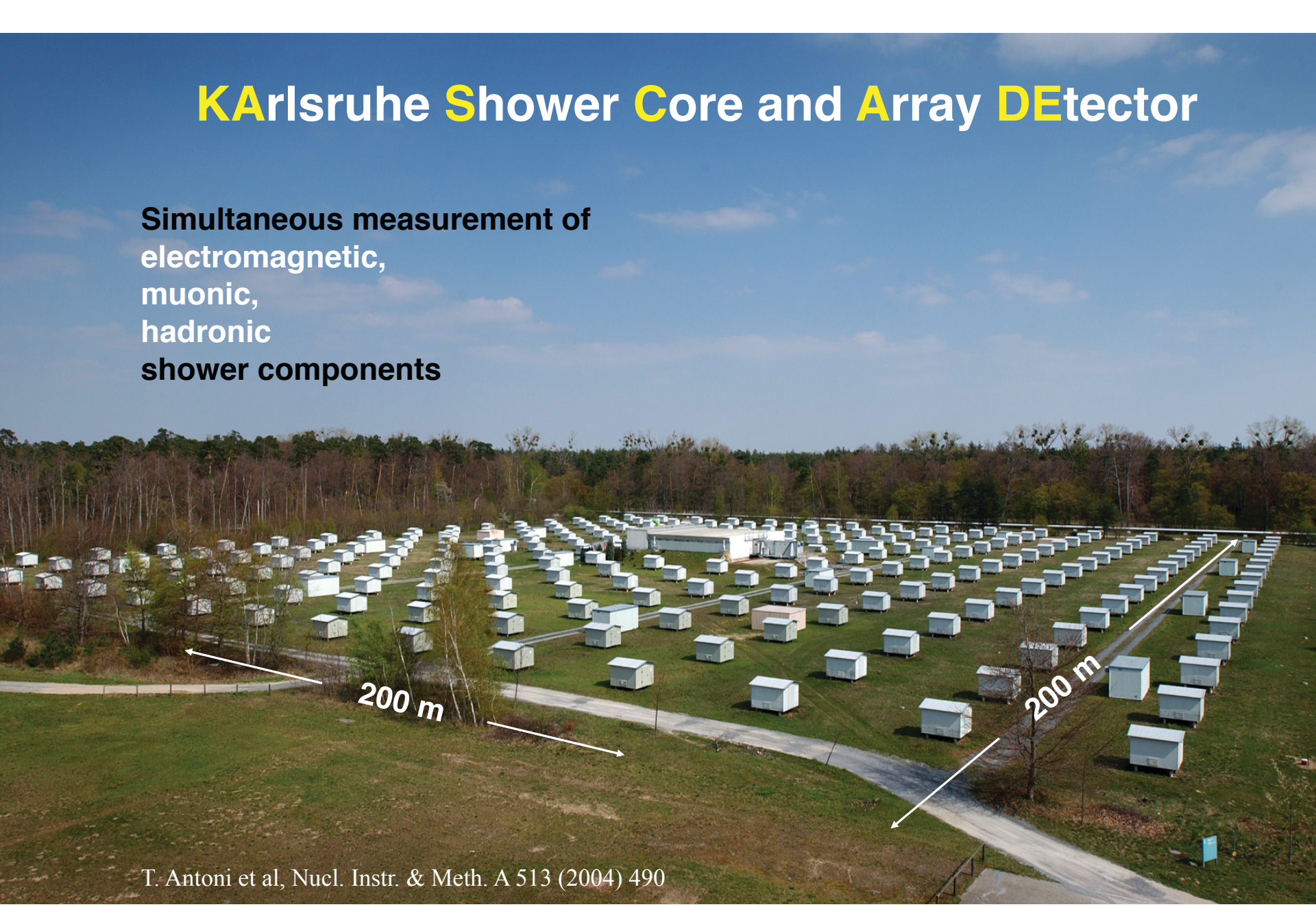

T. Antoni et al, Nucl. Instr. & Meth. A 513 (2004) 490

KArlsruhe Shower Core and Array DEtector

Simultaneous measurement of
electromagnetic,
muonic,
hadronic
shower components

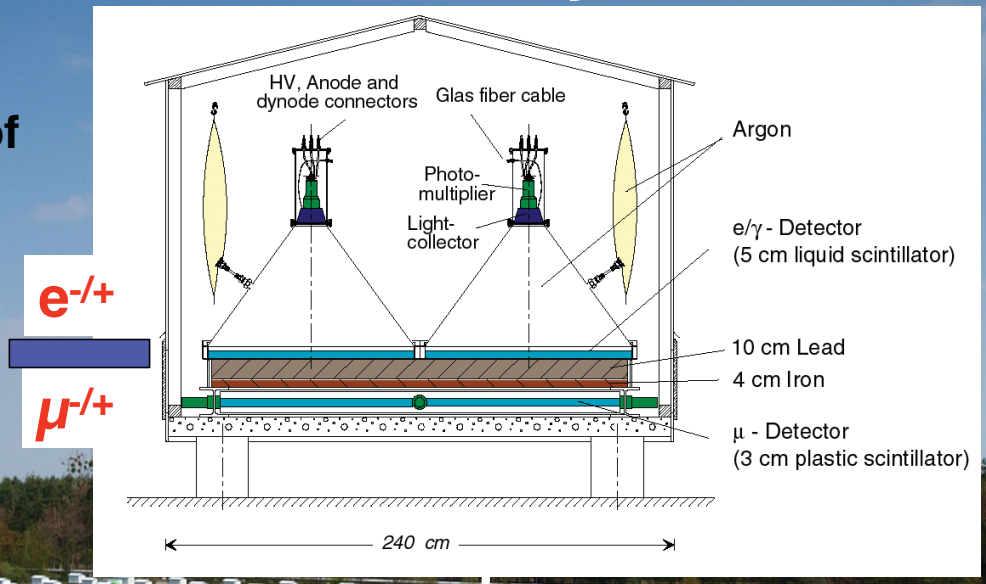

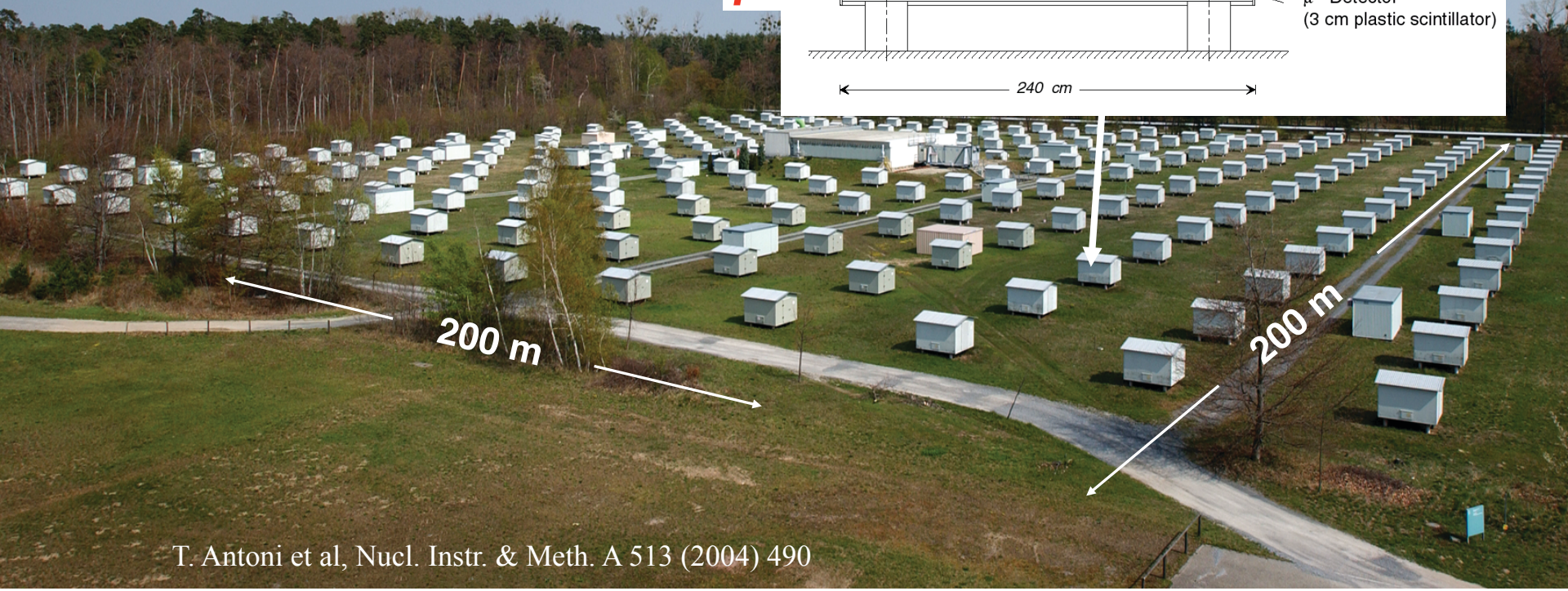

T. Antoni et al, Nucl. Instr. & Meth. A 513 (2004) 490

Event reconstruction in the scintillator array

electromagnetic component

shower core	$\Delta r = 2.5 - 5.5$ m
shower direction	$\Delta\theta = 0.5° - 1.2°$
shower size	$\Delta N_e/N_e = 6 - 12$ %

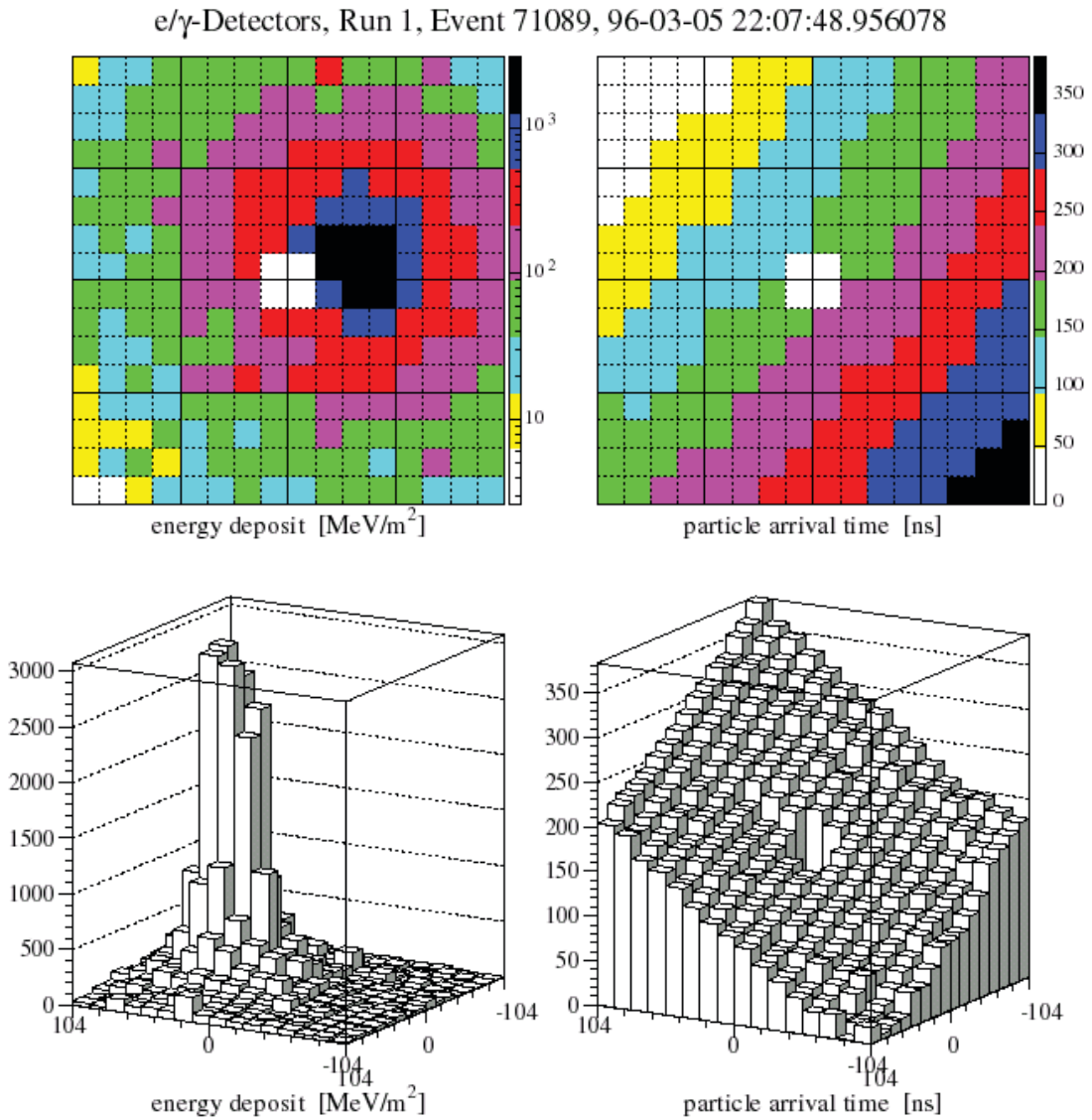

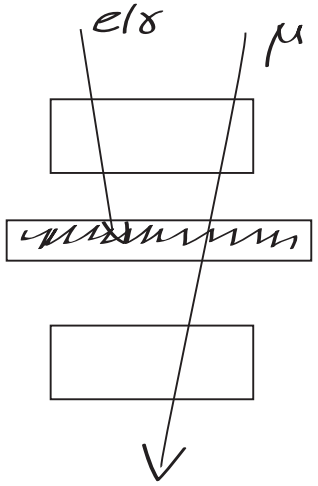

e/γ **detector**

Fe+Pb absrober

μ **detector**

--> count the number of electrons and muons

<u>measurement of hadrons</u>
hadron calorimeter

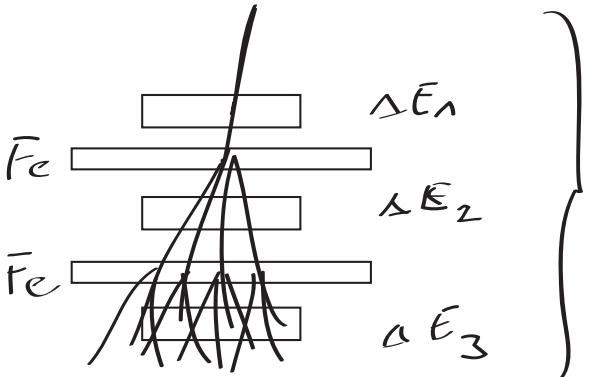

$$\left.\begin{array}{l} \\ \approx 10\lambda_I \\ \\ \lambda_I = \dfrac{1}{n \cdot \sigma} \approx 16.7 \text{ cm} \end{array}\right\}$$ **in Fe**

KASCADE Hadron Calorimeter

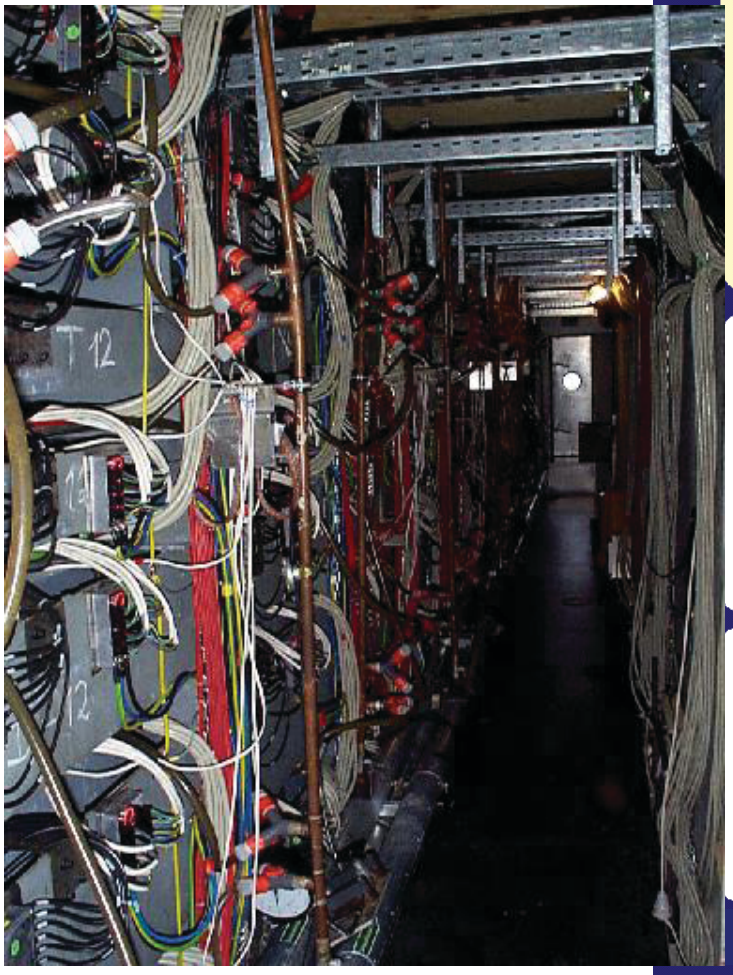

KASCADE Hadron-Calorimeter

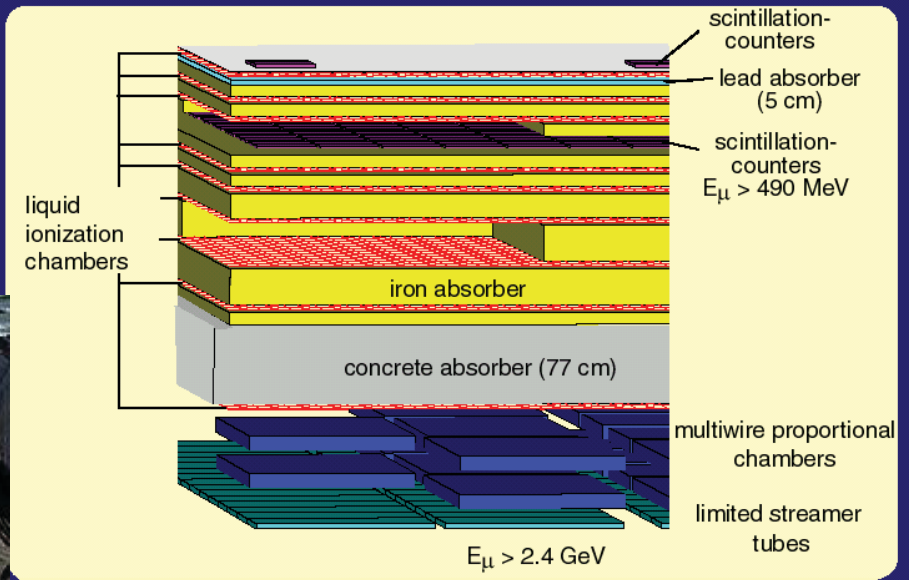

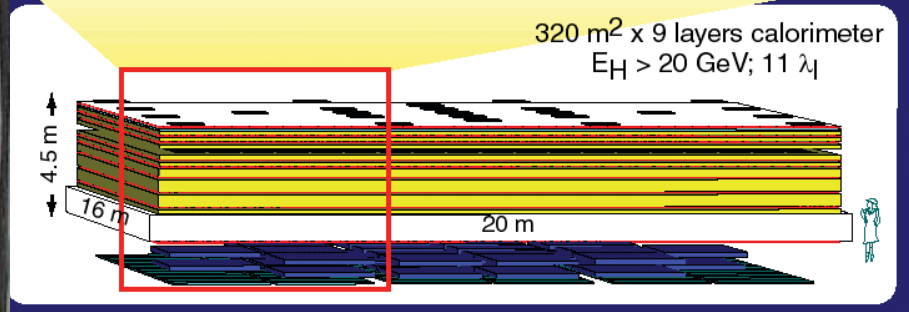

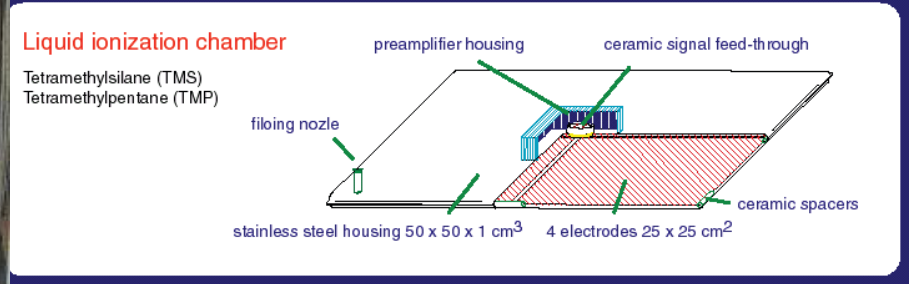

J. Engler et al., Nucl. Instr. Meth. A 427 (1999) 528

Reconstruction of hadrons

Unaccompanied hadron
E_H = 6.6 TeV

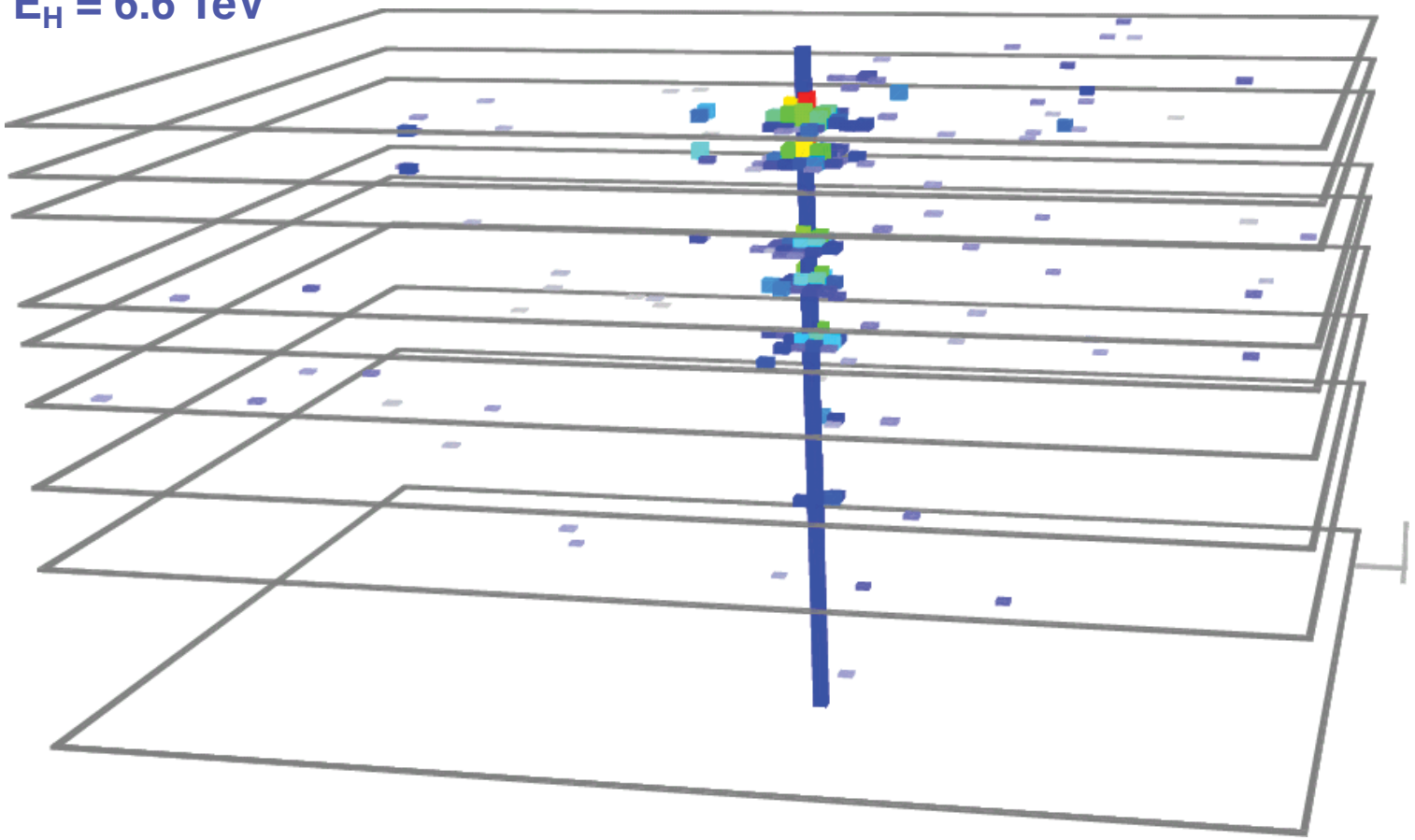

spatial resolution:
Δ_x ~ 10 – 12 cm

angular resolution:
Δ_Ω ~ 1° - 3°

energy resolution:

$$\frac{\sigma(E)}{E}[\%] \approx \frac{250}{\sqrt{E/\ GeV}}$$

Hadronic shower core

$E_0 \sim 6$ PeV

Number of reconstructed hadrons $N_h = 143$

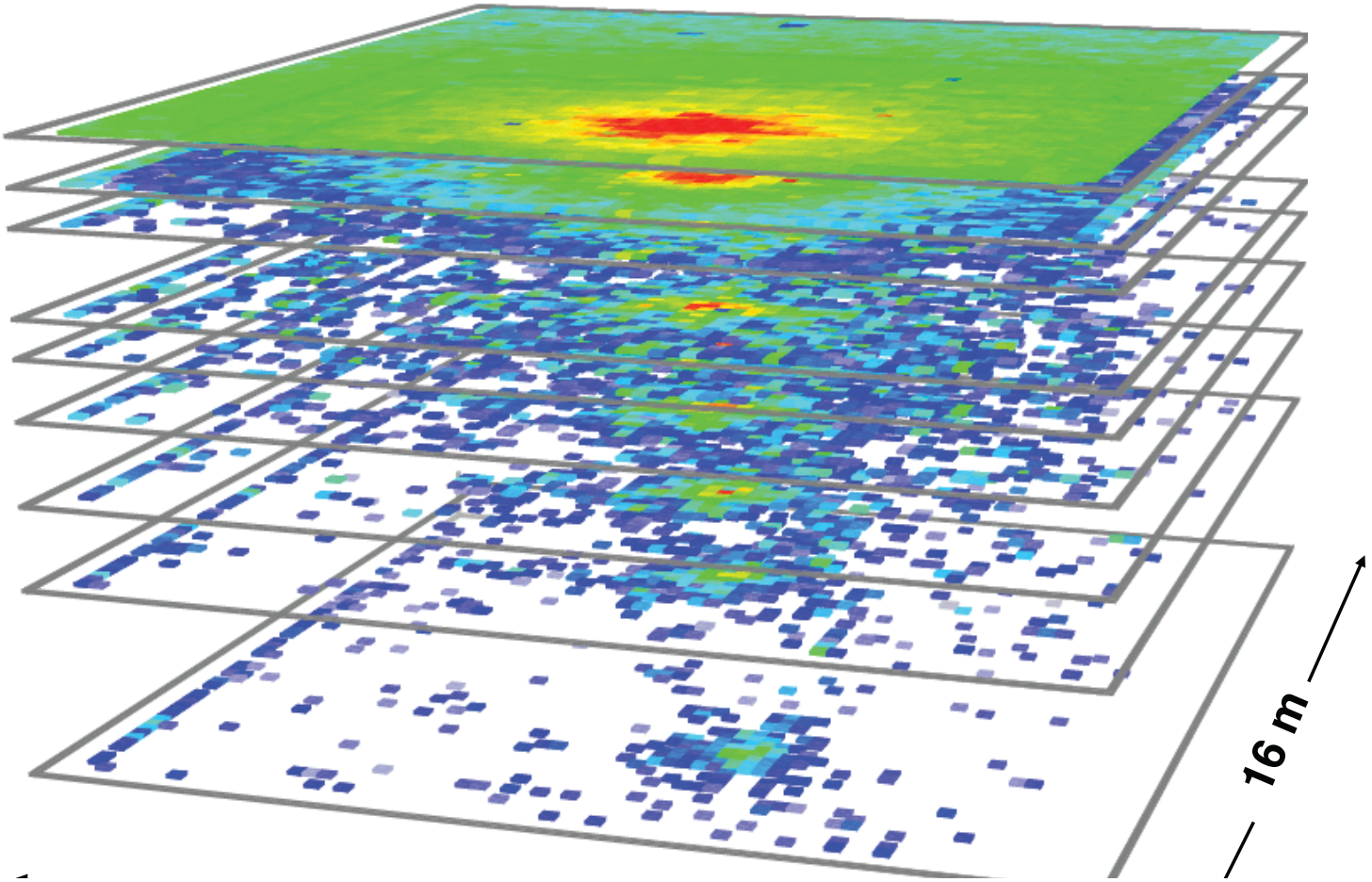

Hadronic shower core

$E_0 \sim 6$ PeV

Number of reconstructed hadrons $N_h = 143$

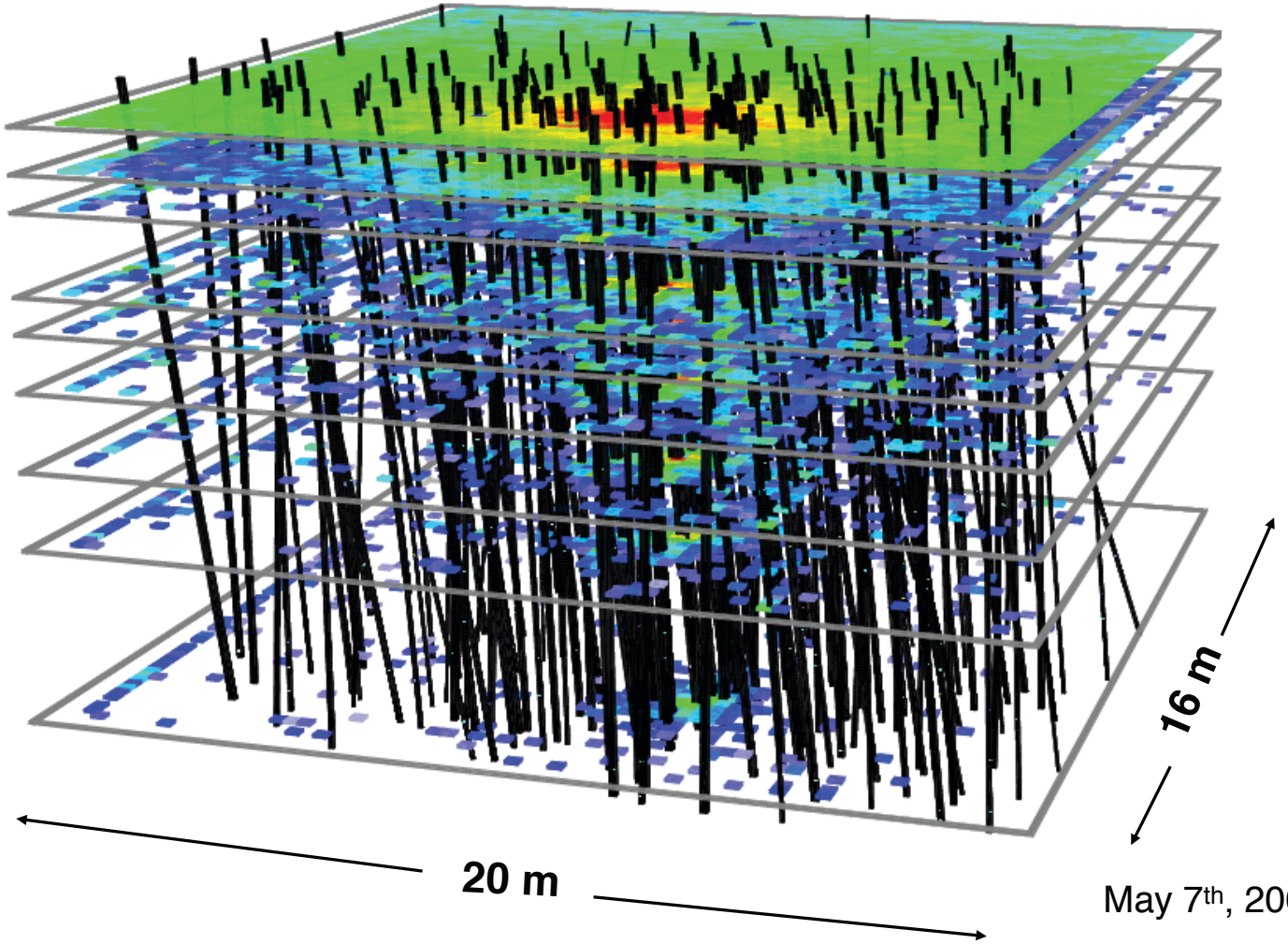

May 7th, 2002 9:45

to determine the properties of the primary particle, we measure the number of

- electrons N_e

- muons N_μ

- hadrons N_h

--> measure the lateral density distribution $\rho_{e,\mu,h}(r)$

$$N_{e,\mu,h} = \int_0^\infty 2\pi r \rho_{e,\mu,h}(r) dr$$

we need a suitable parametrization

$$\rho(r) \propto \left(\frac{r}{r_M}\right)^{s-2} \left(1 + \frac{r}{r_M}\right)^{s-4.5}$$

r_M: Molière radius = 0.25 X_0

in air ~80 m for electrons (analytically derived)
~400 m for muons (empirical)
~15 m for hadrons (empirical)

ELSEVIER

Astroparticle Physics 14 (2001) 245–260

Astroparticle Physics

www.elsevier.nl/locate/astropart

Electron, muon, and hadron lateral distributions measured in air showers by the KASCADE experiment

KASCADE Collaboration

. Perhaps trivial, although experimentally very important, is the fact that in measurements, the shower particles are always sampled over a limited range of core distances $r_1 < r < r_2$ only – in most cases, with an area coverage in this range not much exceeding 1% – while showers are often referred to in terms of integrated numbers of particles,

$$N = \int_{r_1}^{r_2} 2\pi r \rho(r) \mathrm{d}r. \quad (1)$$

The total particle numbers, N, for different kinds and energy ranges of shower particles are obtained by choosing $r_1 = 0$ and $r_2 = \infty$ and are traditionally used both as measures for the primary energy in an individual experiment as well as a means for comparison of different experiments.

Greisen also noted that Eq. (2), except for the last factor, is a close approximation to the analytical calculations for electromagnetic showers performed by Kamata and Nishimura [3] if a shower *age parameter* of $s = 1.25$ is assumed. Greisen's approximation to the Nishimura–Kamata functions for $0.5 < s < 1.5$ is referred to as the NKG function:

$$\rho_{\mathrm{NKG}}(r, s, N_{\mathrm{e}}) = \frac{N_{\mathrm{e}}}{r_{\mathrm{M}}^2} \frac{\Gamma(4.5 - s)}{2\pi\Gamma(s)\Gamma(4.5 - 2s)} \times \left(\frac{r}{r_{\mathrm{M}}}\right)^{s-2} \left(1 + \frac{r}{r_{\mathrm{M}}}\right)^{s-4.5}. \quad (3)$$

This function, often used to describe the charged particle lateral distribution, will in the following be applied individually to electron, muon, and hadron distributions by choosing approriate sets of parameters (s, r_{M})

Deviations of the experimental LDF from the NKG function (Eq. (3)) have been discussed in the literature frequently (Section 1) and are subject to more detailed studies presented below. It turns out that the NKG function can describe the KASCADE electron LDF over the core distance range 10–200 m surprisingly well, but the best agreement is achieved with parameters far away from the conventional assumption of $r_M \approx 80$ m. When fitting N_e, r_M, and s simultaneously, the measured LDFs can be reproduced at the 1% level for $r_M \approx 20$–30 m and $s \approx 1.6$–1.8.

T. Antoni et al. / Astroparticle Physics 14 (2001) 245–260

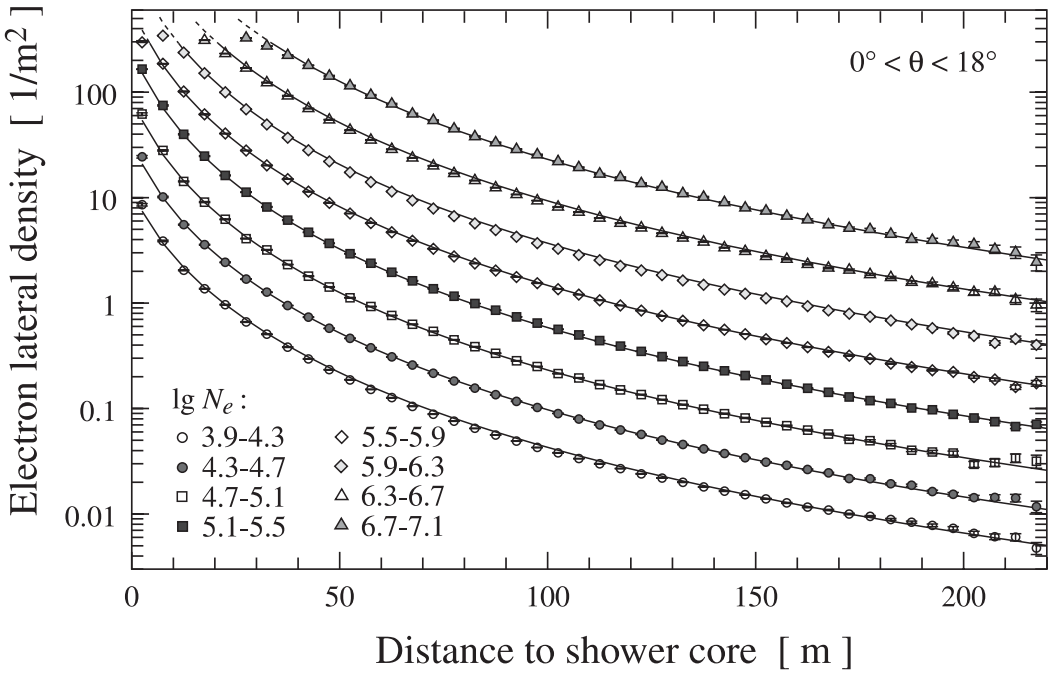

Fig. 2. Lateral distributions of electrons above a 5 MeV kinetic energy for zenith angles below 18°. The lines show NKG functions of fixed age parameter $s = 1.65$ but varying scale radius r_e (see the text).

Table 1
KASCADE detector components used in this analysis[a]

Detector	Channels	Separation (m)	Total area (m^2)	Threshold E_{kin}	Particle
Array e/γ	252	13	490	5 MeV	e
Array μ	192	13	622	230 MeV $\times$ sec θ	μ
Trigger	456	–	208	490 MeV $\times$ sec θ	μ
MWPCs	26 080	–	129	2.4 GeV $\times$ sec θ	μ
Calorimeter	38 368	–	304	50 GeV	Hadrons

[a] Detection thresholds refer to the particle energies above the absorber material of the detectors.

5. Muon lateral distributions

The KASCADE experiment measures lateral distributions of muons for three different energy thresholds (Table 1). In the following, we group the showers in bins of truncated muon numbers N_μ^{tr}. Punch-through and efficiency corrections are applied as described in Section 3. Ranges of core distances for the different muon energy thresholds are limited by the uncertainties in the punch-through corrections at small core distances and by the geometry of the KASCADE detector array. Since N_e/N_μ^{tr} rises with the shower size, the impact of punch-through corrections becomes more severe at higher energies and the minimum core distances have to be increased correspondingly. For showers with cores inside KASCADE, the upper limit is about 220 m for array detectors and 100 m for central detector components.

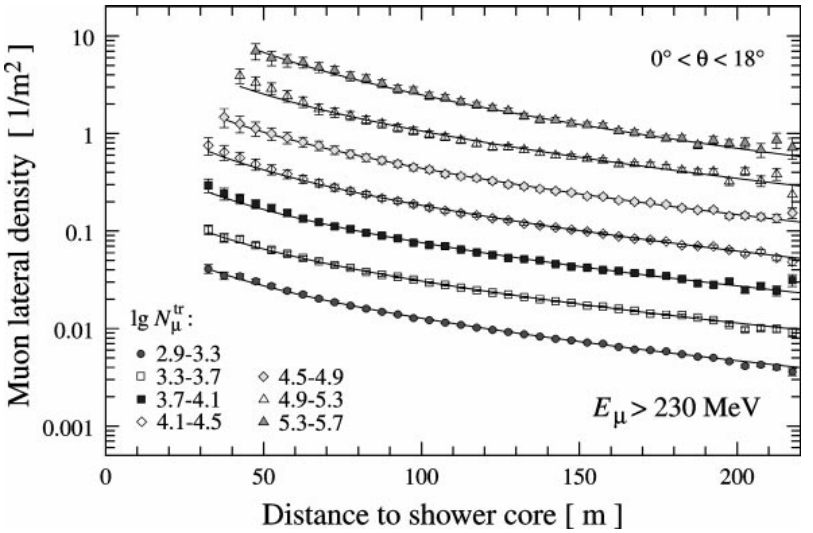

Fig. 7. Lateral distribution of muons above 230 MeV kinetic energy measured with the array detectors. The lines indicate NKG functions fitted to the data. Error bars are of statistical nature including an uncertainty of 10% on the punch-through correction applied.

NKG functions with $r_\mu = 420$ m

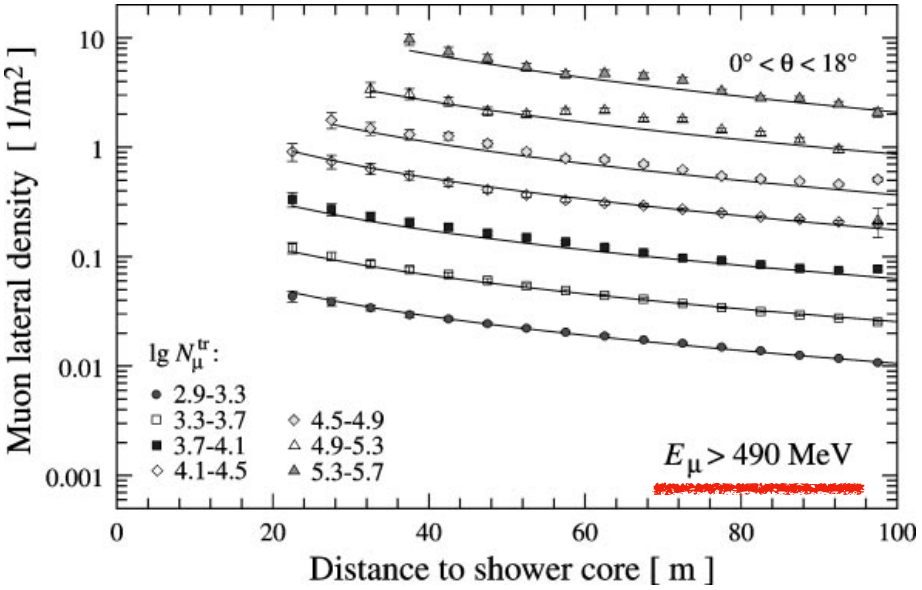

Fig. 8. Lateral distribution of muons above 490 MeV kinetic energy as measured with the trigger plane. Data are binned according to N_μ^{tr} as measured by the array and the lines represent NKG fits to the data.

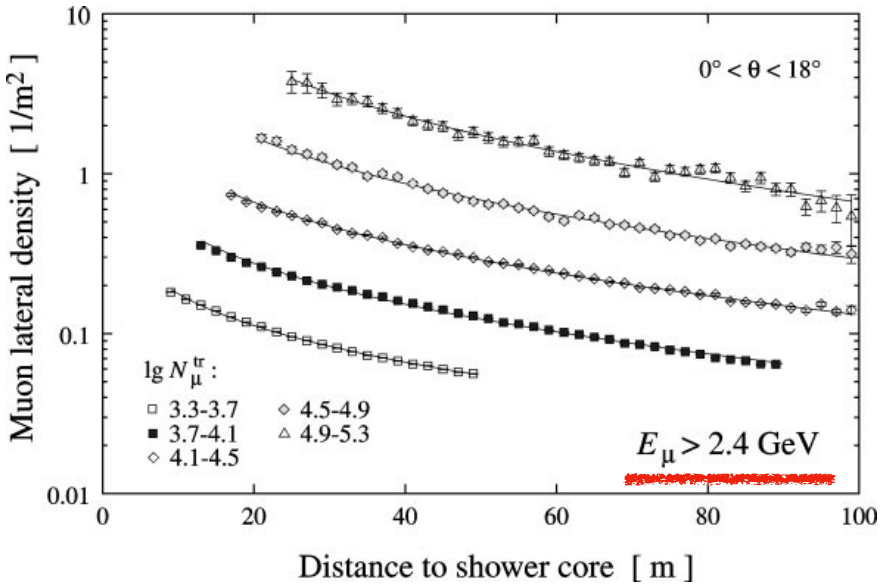

Fig. 9. Lateral distribution of muons above 2.4 GeV kinetic energy. Error bars are statistical only. Data are binned according to N_μ^{tr} as measured by the array and the lines represent NKG fits to the data.

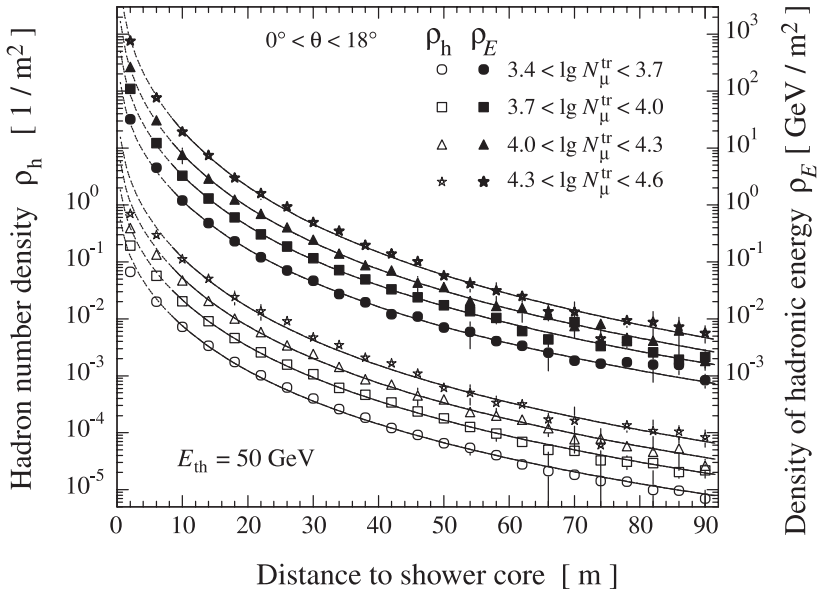

Fig. 12. Density of hadron number (left scale, open symbols) and of hadronic energy (right scale, filled symbols) versus the core distance for showers of truncated muon numbers as indicated. Threshold energy for hadrons is 50 GeV. The curves represent fits of the NKG formula to the data at $r \geqslant 8$ m with a radius fixed to $r_h = 10$ m.

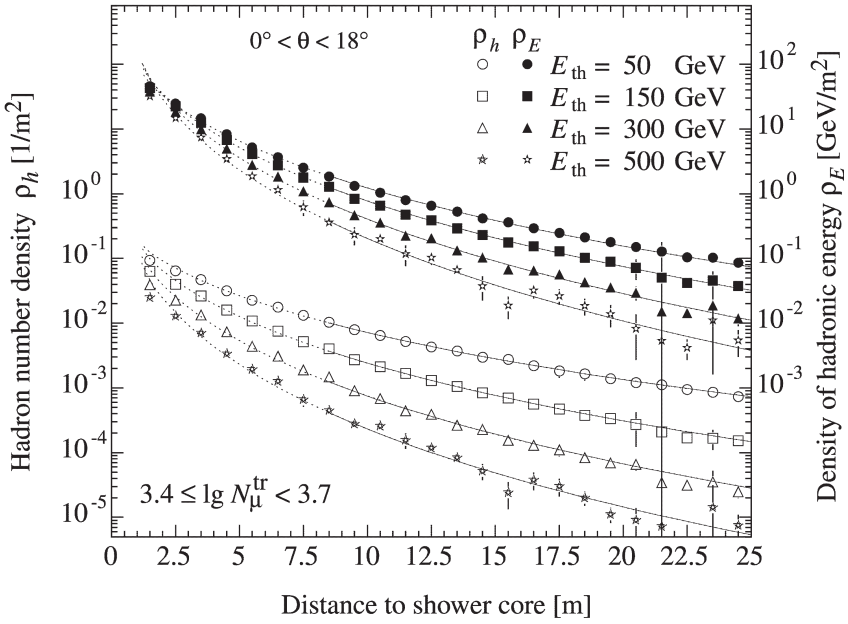

Fig. 14. Density of hadron number (left scale, open symbols) and of hadronic energy (right scale, filled symbols) versus shower core distance for various thresholds of hadron energy. The curves represent fits of the data to the NKG function as in Fig. 12.

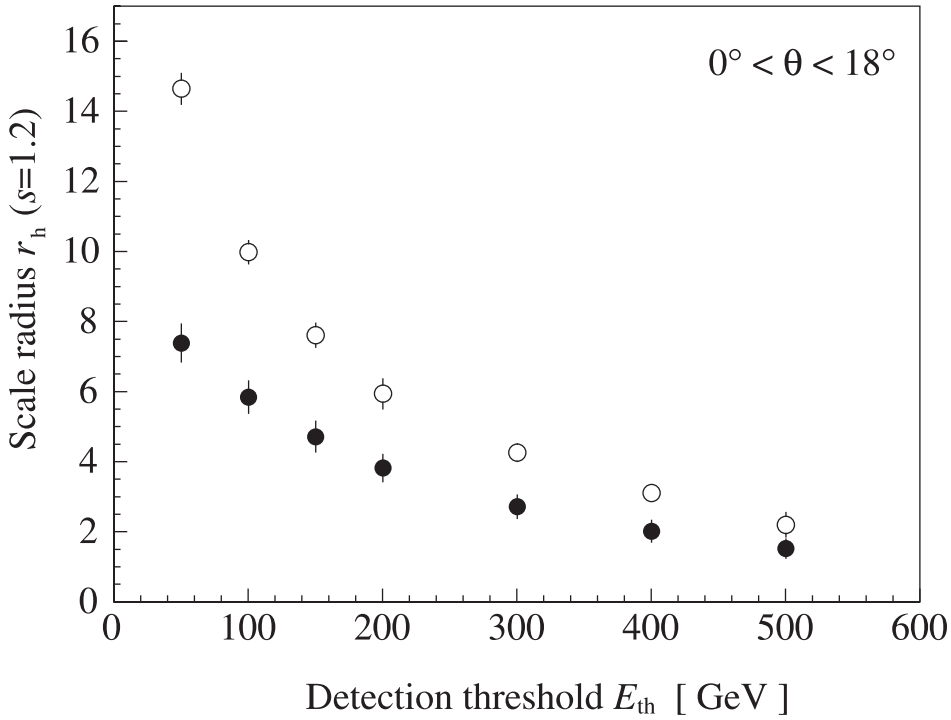

Fig. 15. Hadronic scale radius r_h as a function of detection threshold E_{th} for a fixed shower age of $s = 1.2$ and $3.4 < \lg N_\mu^{tr} < 3.7$. Filled symbols are for hadronic energy density and open symbols for hadronic particle density.

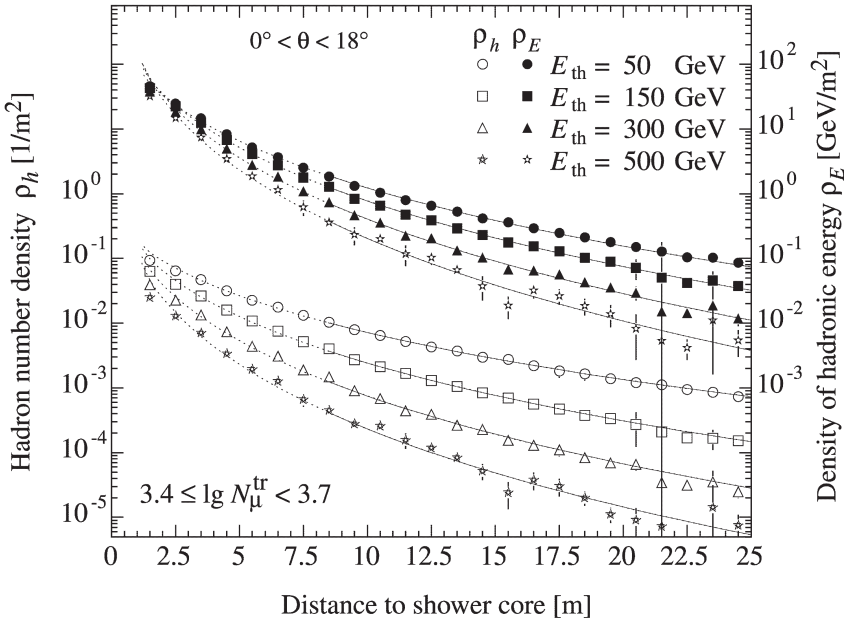

Fig. 14. Density of hadron number (left scale, open symbols) and of hadronic energy (right scale, filled symbols) versus shower core distance for various thresholds of hadron energy. The curves represent fits of the data to the NKG function as in Fig. 12.

The core position of the shower is found by fitting the signal $S(r)$ of the detector stations with a lateral distribution function (LDF) tailored for the response of the particular array. The parameters of the lateral distribution can be determined from data directly using vertical showers. Because the NKG function (Eq. 15.35) was developed to describe EM showers only, various modified versions have been developed to describe the charged particles in more complex hadronic showers. An example of a modified NKG form is

$$\rho_e\,(m^{-2}) = f(x) = C_1(s)\,x^{(s-2)}(1+x)^{(s-4.5)}\,(1 - C_2\,x^d), \qquad (16.29)$$

where $x = r/r_1$, and the normalization constant is[3]

$$C_1(s) = \frac{N_e}{2\pi r_1^2}[B(s, 4.5-2s) + C_2\,B(s-d, 4.5-d-2s)]^{-1}.$$

The scale for the NKG lateral distribution function is the Molière unit, which at the depth of the Akeno array of 920 g/cm^2, for example, is $r_1 \approx 85$ m. For showers of size $N_e \approx 10^6$ at sea level, Greisen [538] uses $s = 1.25$, $d = 1$ and $C_2 = 0.088$. Nagano et al. [539] at 920 g/cm^2 use $d = 1.3$ and $C_2 = 0.2$ with s fitted for each shower. The modified NKG form used for the surface array of Auger is

$$S(r) = \tilde{C}\left(\frac{r}{r_s}\right)^{-\beta}\left(1+\frac{r}{r_s}\right)^{-\beta}. \qquad (16.30)$$

A list of often-used LDF parametrizations can be found in [540]. In general, one of the fitting parameters accommodates fluctuations in shape while another characterizes the density at a particular distance, r_s.

For arrays that can separate muons from $e^{\pm}$ it is useful to have a separate lateral distribution function tailored for the somewhat flatter muon distribution. A standard form is due to Greisen [538]:

$$\rho_\mu(\mathrm{m}^{-2}) = \frac{\Gamma(2.5)}{2\pi\Gamma(1.25)\Gamma(1.25)} \left(\frac{1}{320}\right)^{1.25} N_\mu r^{-0.75} \left(1+\frac{r}{320}\right)^{-2.5}. \tag{16.31}$$

The distribution is normalized so that N_μ is the total number of muons in the shower at the surface.

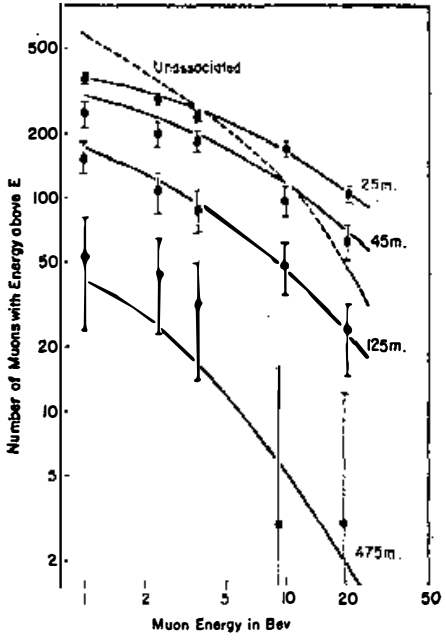

FIG. 4. Mu-meson energy spectra at various distances from extensive air-shower axes, measured by Bennett (8). The data cover a wide range of shower sizes, $10^3 < N < 10^7$, and each solid curve refers to a considerable interval of radius, with mean values indicated. The dashed curve refers to mesons that were not coincident with detected showers. The solid curves were computed with the following expression for the density of mesons (per sq. m.) with energy above E (Bev) at distance r(m.) from the axis of showers containing N charged particles:

The Pierre Auger Observatory

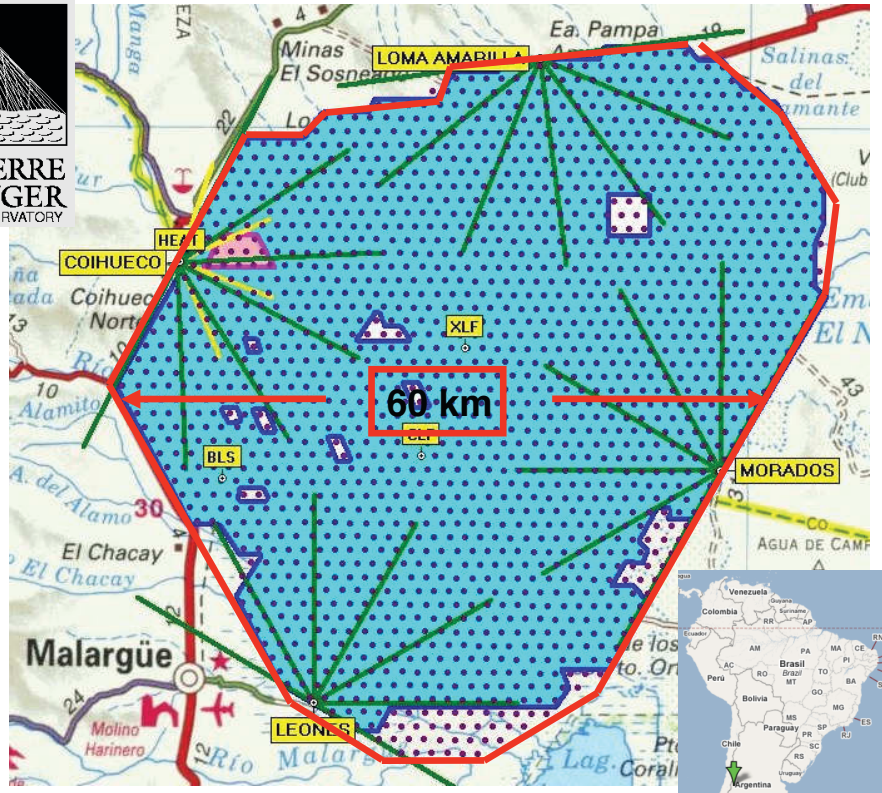

3000 km²
1661 water Cherenkov detectors
24+3 Fluorescence telescopes
~150 radio antennas

The detection principle

ΔE = 18% stat. 22% syst.
ΔΘ < 1°

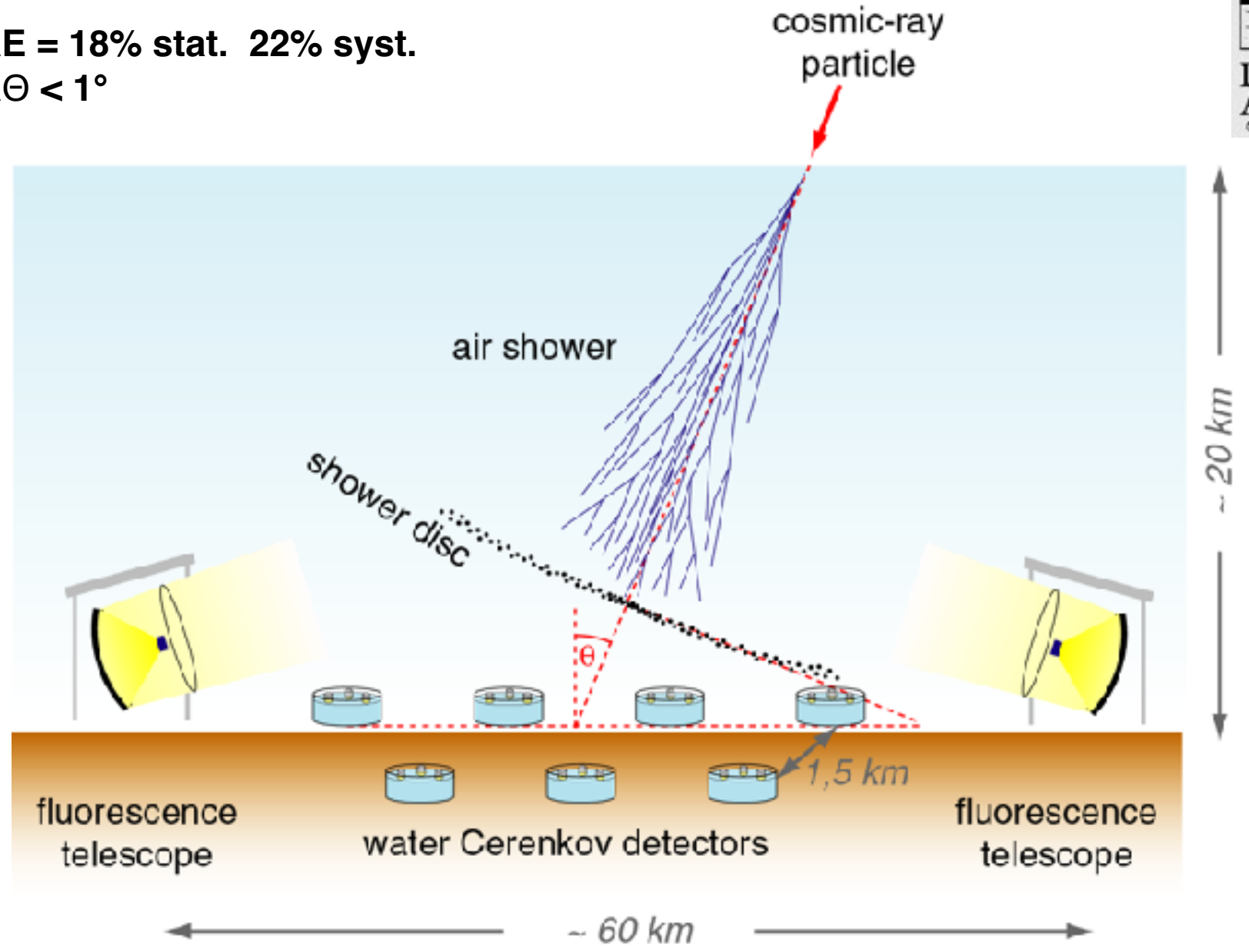

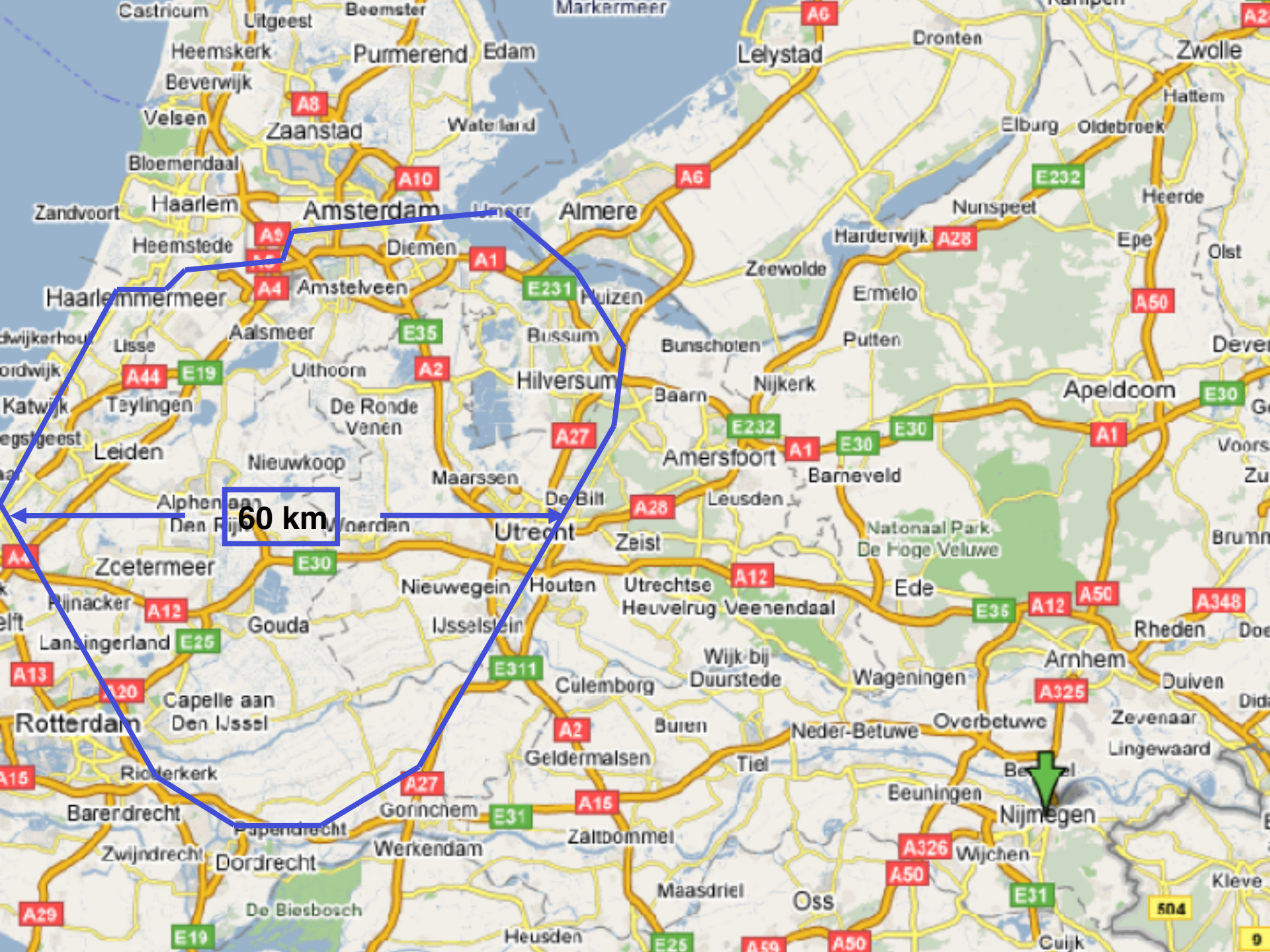
60 km
Castricum
Uitgeest
Beemster
Markermeer
Heemskerk
Purmerend
Edam
Lelystad
Dronten
Zwolle
Beverwijk
Velsen
Zaanstad
Waterland
Hattem
Elburg
Oldebroek
Bloemendaal
Haarlem
Amsterdam
Almere
Zandvoort
Nunspeet
Heerde
Heemstede
Diemen
Harderwijk
Epe
Olst
Haarlemmermeer
Amstelveen
Zeewolde
Ermelo
Aalsmeer
Bussum
Bunschoten
Putten
Lisse
Uithoorn
Hilversum
Nijkerk
Apeldoorn
Katwijk
Teylingen
De Ronde Venen
Baarn
Leiden
Nieuwkoop
Amersfoort
Barneveld
Maarssen
De Bilt
Leusden
Alphen aan Den Rijn
Woerden
Utrecht
Zeist
Nationaal Park De Hoge Veluwe
Zoetermeer
Nieuwegein
Houten
Utrechtse Heuvelrug
Veenendaal
Ede
Rijnacker
Gouda
IJsselstein
Rheden
Lansingerland
Wijk bij Duurstede
Arnhem
Culemborg
Wageningen
Duiven
Rotterdam
Capelle aan den IJssel
Overbetuwe
Zevenaar
Buren
Neder-Betuwe
Lingewaard
Geldermalsen
Tiel
Ridderkerk
Beuningen
Barendrecht
Gorinchem
Nijmegen
Papendrecht
Zaltbommel
Zwijndrecht
Dordrecht
Werkendam
Wijchen
Maasdriel
Oss
De Biesbosch
Heusden
Cuijk
A6
A8
A10
A9
A1
A4
A44
A2
A27
A28
A12
A50
A348
A325
A326
A15
A13
A20
A29
E231
E35
E19
E232
E30
E311
E25
E31

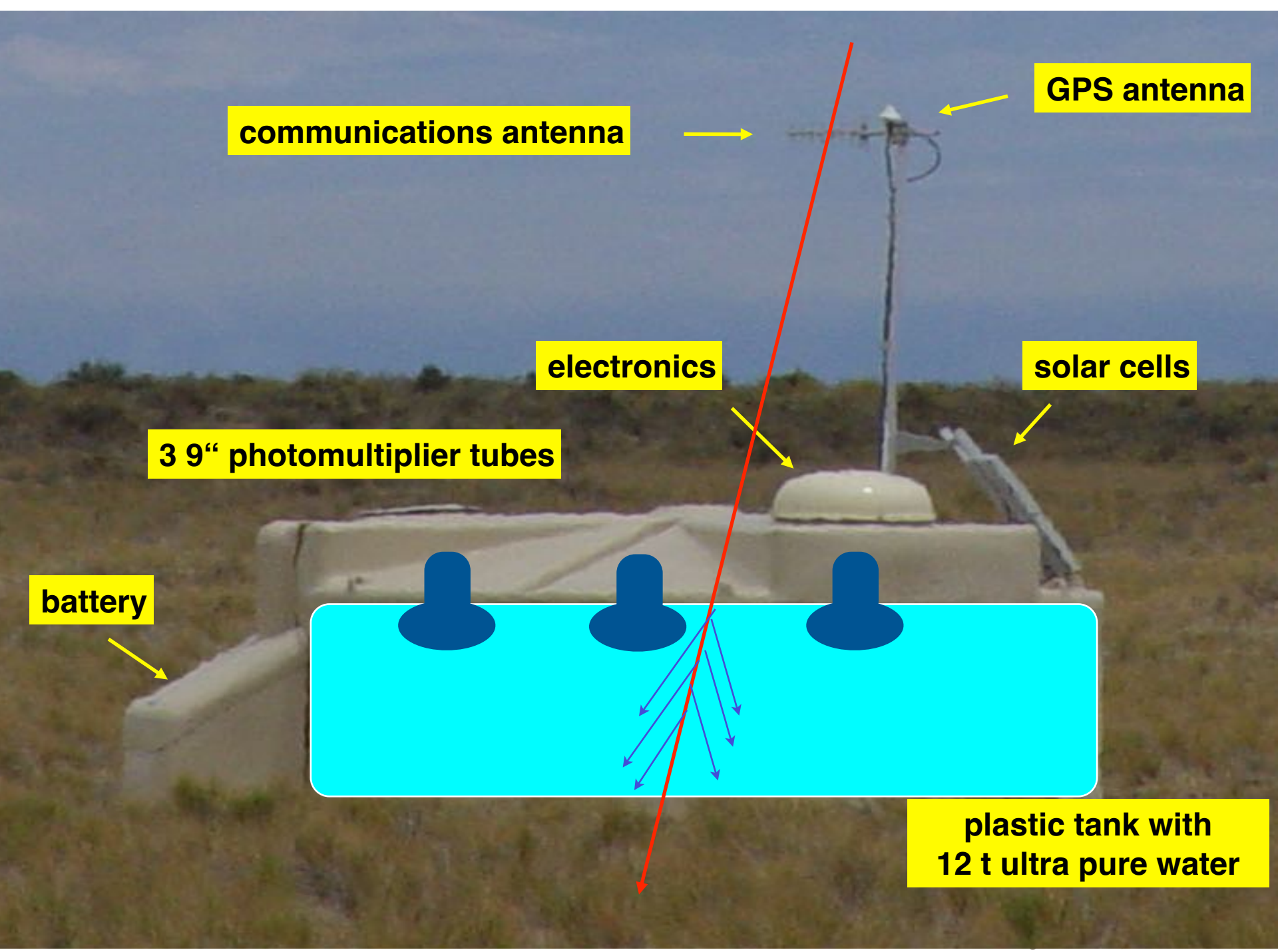
communications antenna
GPS antenna
electronics
solar cells
3 9“ photomultiplier tubes
battery
plastic tank with
12 t ultra pure water

Air shower registered with water Cherenkov detectors

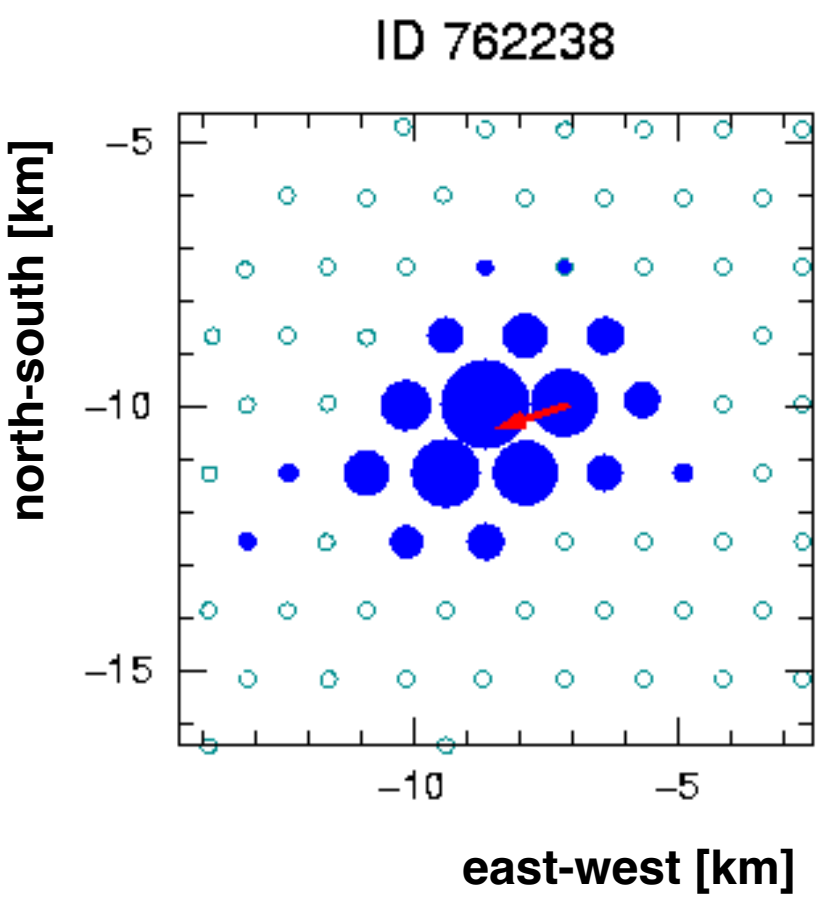

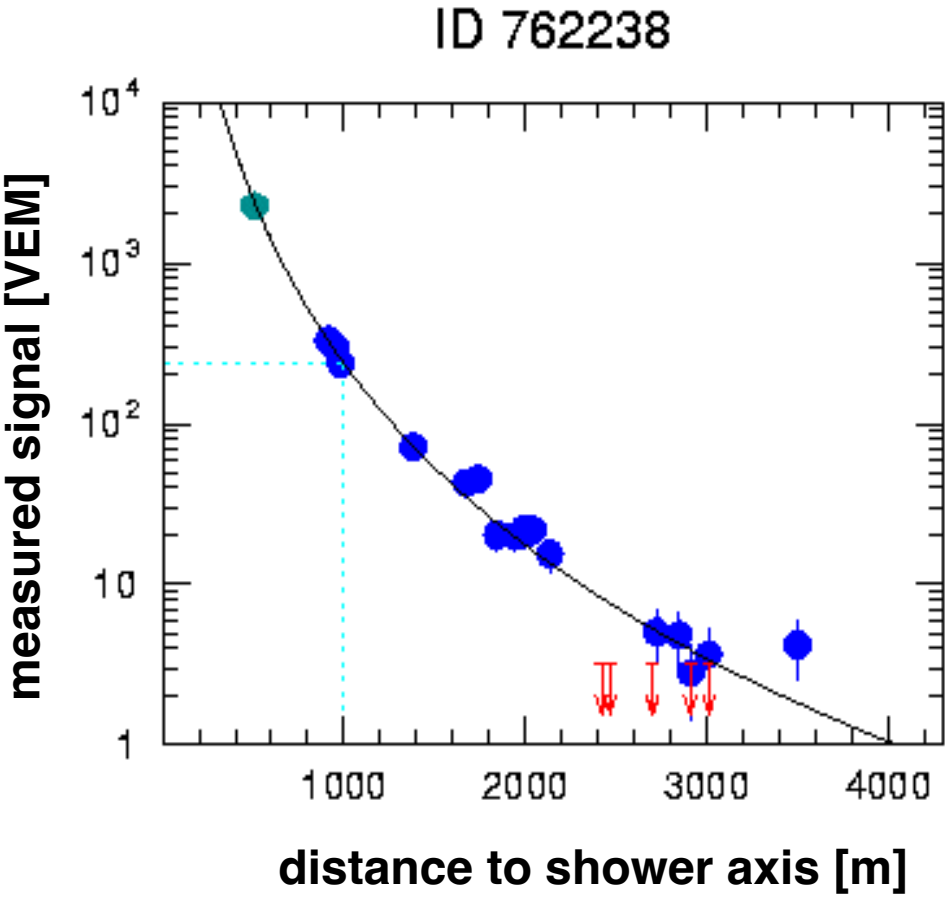

To reconstruct the energy of a shower, a measured ground parameter is defined. Examples are the number of detected particles at ground calculated by integrating the lateral distribution or a signal density at a specific lateral distance. The latter is illustrated in Figure 16.5 for the Auger surface detector array. The measured signals of the detector stations of one particular event are reconstructed with the LDF of Eq. 16.30 with different values of β. A fix point is found at a core distance of about $r_{\mathrm{opt}} = 1100\,\mathrm{m}$ [541]. The signal (i.e. particle density) obtained for this distance is independent of the details of the LDF used for reconstruction and, hence, can be used as a robust estimator for determining the shower energy through comparison with Monte Carlo reference showers or cross-calibration with other calorimetric energy measurements. The optimum distance depends mainly on the spacing of the detectors and is not related to shower-to-shower fluctuations.

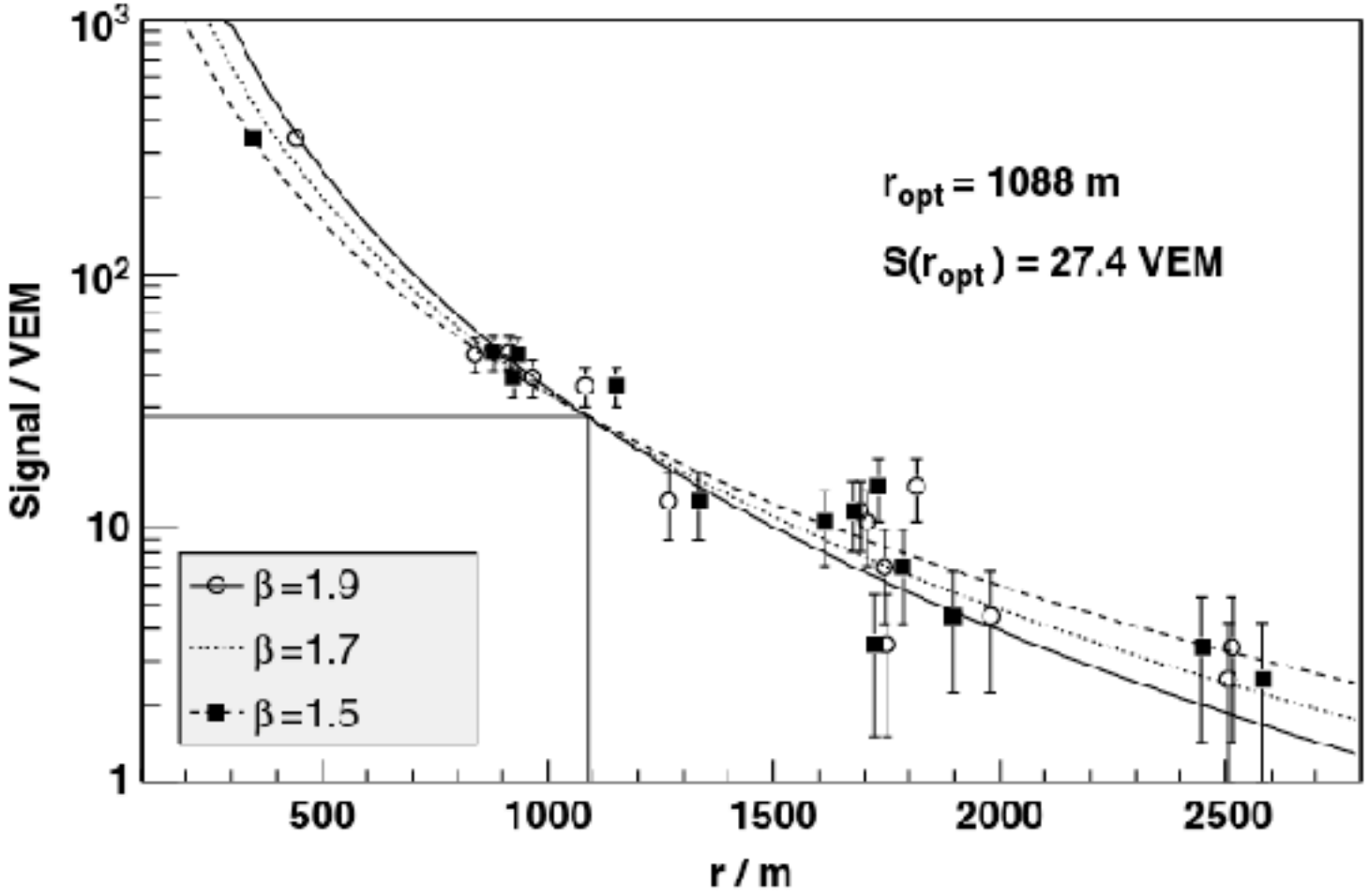

Figure 16.5 Example of the determination of the optimum distance for measuring the particle density of an air shower in the Pierre Auger Observatory (see text). The detector signal is expressed in units of the signal expected for vertical muons (vertical equivalent muons, VEM). From [541].

particle type from air-shower measurements

The most promising surface-detector approach is the separate measurement of the number of electrons and muons. The corresponding predictions for air showers simulated with the hadronic interaction models EPOS [146, 161] and Sibyll [158] (interactions with $E > 80\,\mathrm{GeV}$) and FLUKA [193] (interactions with $E \lesssim 80\,\mathrm{GeV}$) are shown in Figure 16.6. The simulation results confirm the predictions of the superposition model (16.19) with $N_\mu \propto E_0^\alpha$, $\alpha \approx 0.90$ and a relative difference in the muon number between iron and proton showers of $\sim 40\%$. The difference in the number of electrons at each energy is mainly related to the shallower depth of shower maximum of iron showers relative to proton showers.

With the energy transferred to the EM shower component being closely related to (and anti-correlated with) the number of muons at ground, one can devise an almost model-independent estimator for the primary energy

$$E_0 = E_{\mathrm{em}} + E_{\mathrm{had}} \approx \tilde{E}_c N_e^{(\max)} + E_{\mathrm{dec}} N_\mu , \qquad (16.32)$$

where $\tilde{E}_c > E_c$ is a typical energy scale one has to assign to electrons to compensate for the non-detected photons. In practical applications, the energy is parametrized as $\ln E = a \ln N_e + b \ln N_\mu + c$, with a, b, c being parameters determined from simulations. A similar expression can be written for $\ln A$ to find the primary mass; see [540, 544]. Depending on the distance of the observation level to the depth of the typical shower maximum, fluctuations in the particle numbers can be large and need to be accounted for in energy and composition reconstruction.

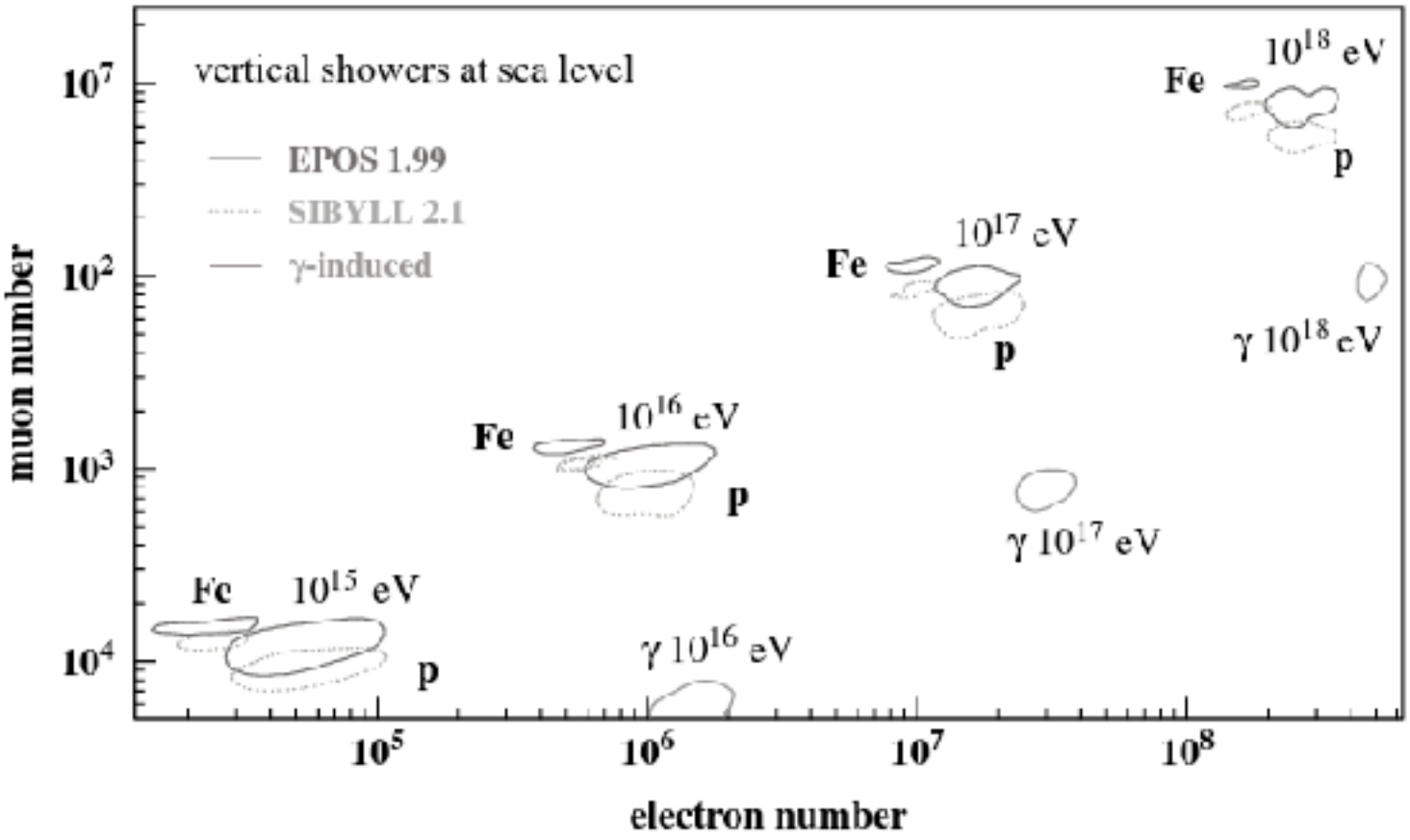

Figure 16.6 Predicted correlation between the number of muons and electrons of vertical showers at sea level. The simulations were done with CORSIKA [640] using the same cutoff energies for the secondary particles as in Figure 16.1. The curves encircle approximately the one-sigma range of the fluctuations. From [33], © 2011 by Annual Reviews (www.annualreviews.org), reproduced with permission.

KASCADE-Grande – Lateral distributions

NKG function

$$\rho(r, s, N_e) = \frac{N_e}{r_M^2} \frac{\Gamma(4.5 - s)}{2\pi\Gamma(s)\Gamma(4.5 - 2s)} \left(\frac{r}{r_M}\right)^{s-2} \left(1 + \frac{r}{r_M}\right)^{s-4.5}$$

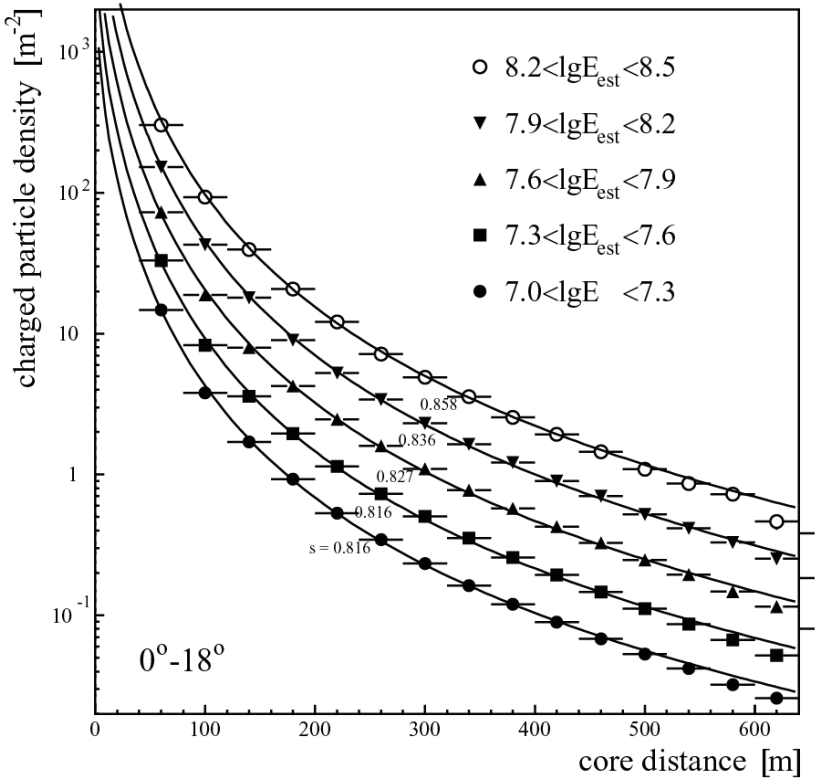

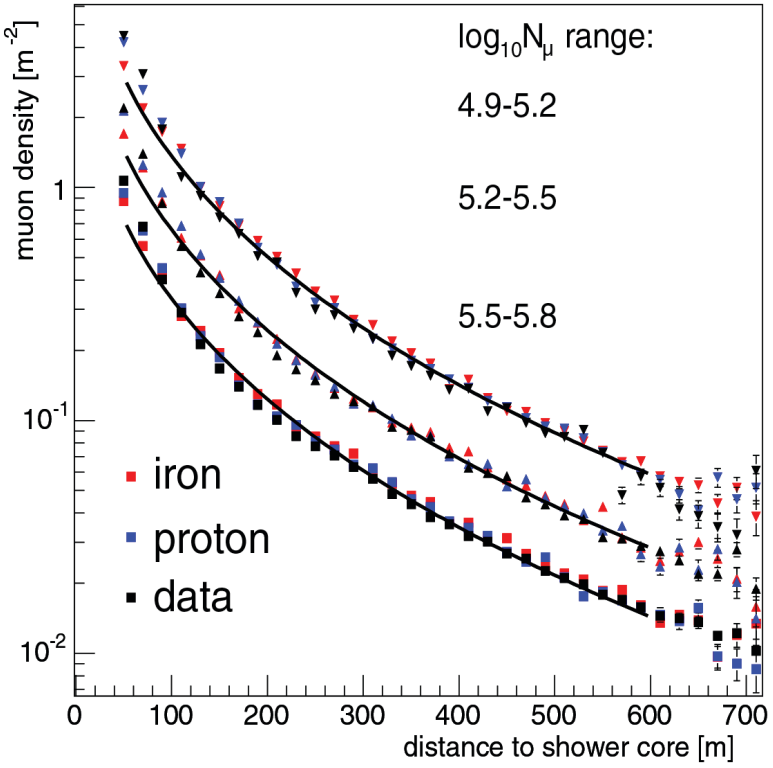

R. Glasstetter et al., Proc. 29th ICRC, Pune 6 (2005) 293

J. v. Buren et al., Proc. 29th ICRC, Pune 6 (2005) 301

KASCADE-Grande – Lateral distributions

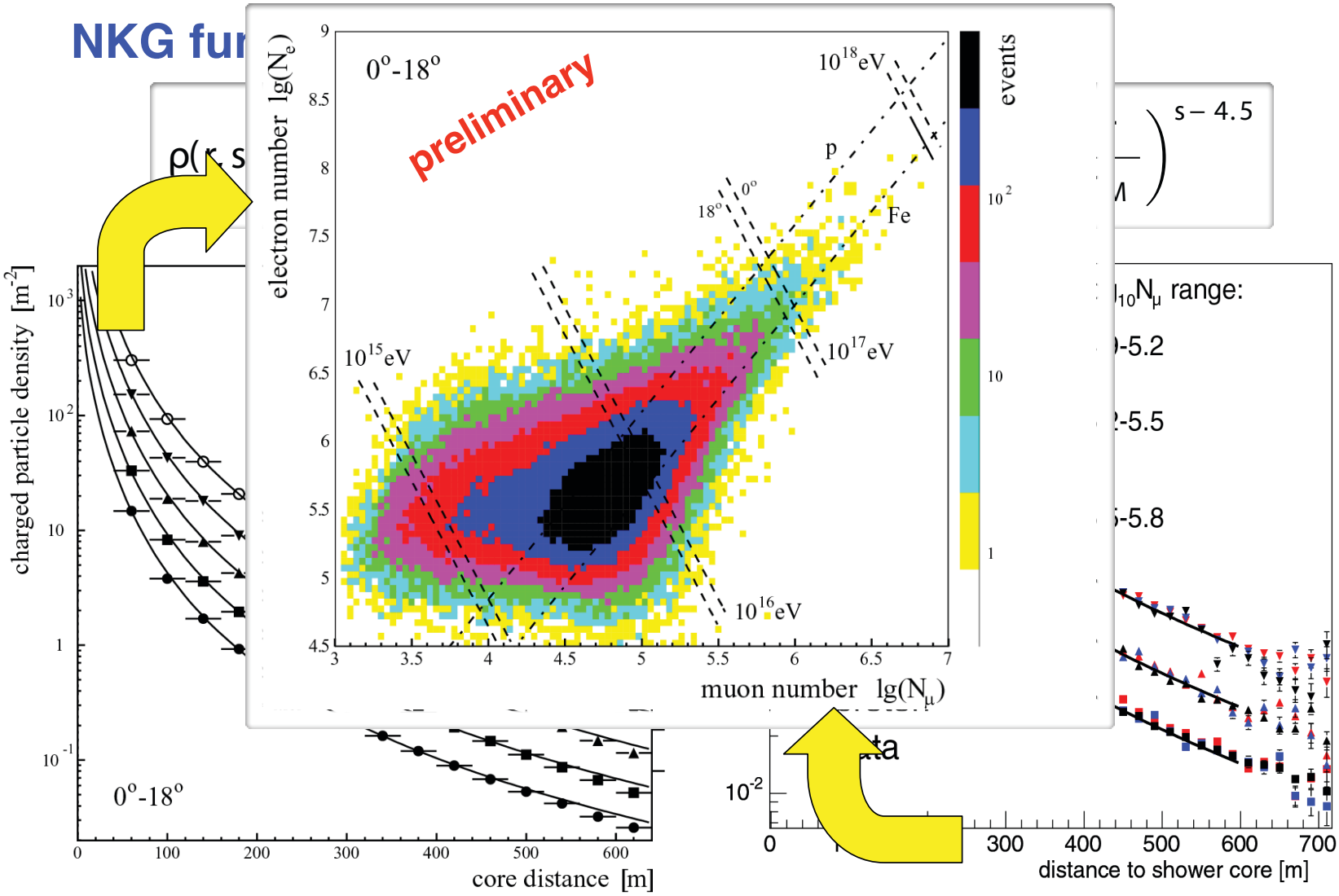

R. Glasstetter et al., Proc. 29th ICRC, Pune 6 (2005) 293

J. v. Buren et al., Proc. 29th ICRC, Pune 6 (2005) 301

to determine the mass of the primary particle

- $\frac{e}{\mu}$ ratio or $\frac{h}{\mu}$ ratio
- muon production height or X_{max} for e/m comp.

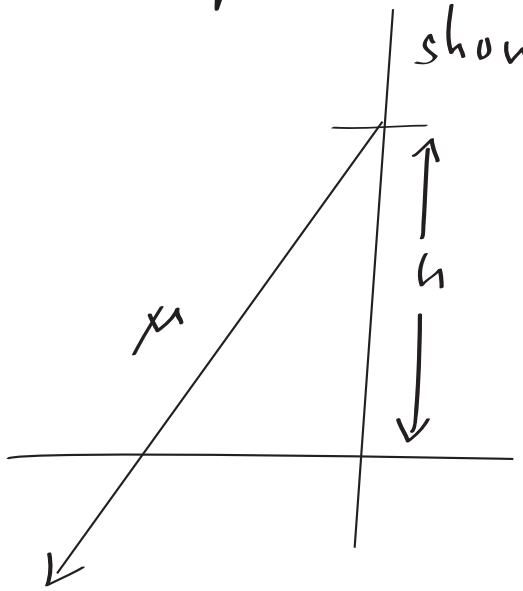

large h → heavy primary particle

small h → light particle

Muon production height – KASCADE muon tracking detector

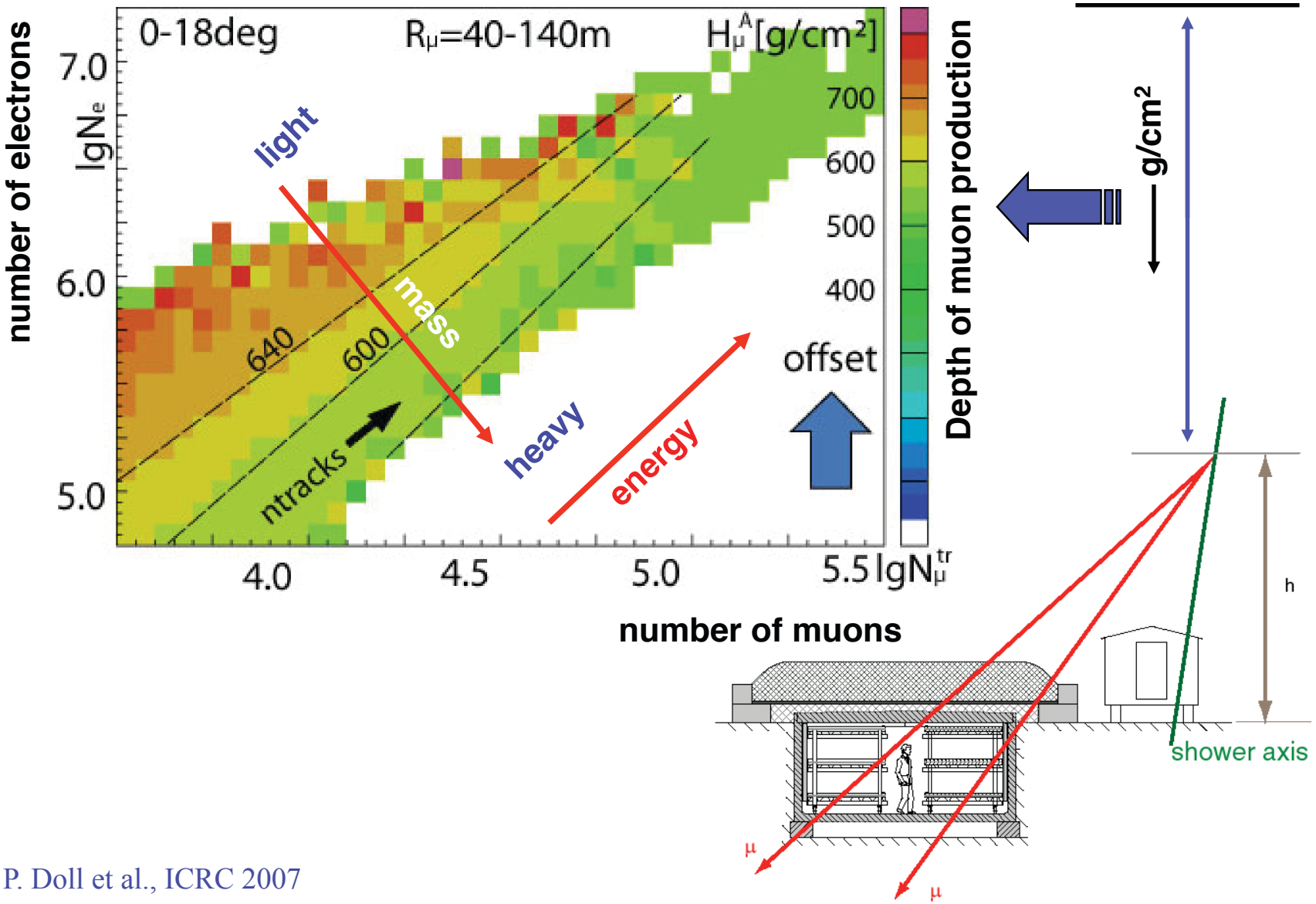

P. Doll et al., ICRC 2007

16.8 Atmospheric Cherenkov light detectors

The large number of Cherenkov photons emitted by charged particles traversing a medium with refractive index $n > 1$ can be used for efficient detection of air showers in a wide range of energies. The atmospheric Cherenkov technique is useful both for γ-ray astronomy and for study of cosmic ray air showers. Imaging atmospheric Cherenkov telescopes (IACTs) can detect showers with thresholds down to 30 GeV [566, 567]. Their reach at high energy, however, is limited to $\sim$ 100 TeV by their relatively small effective area. Non-imaging Cherenkov detectors can be set up similar to an array of particle detectors, offering the possibility to instrument very large areas at ground and reach very high energy [568, 569]. Typically only the Cherenkov light of the abundant secondary particles in an air shower is detected, but also the direct Cherenkov light of the primary particle can be measured [570, 571]. From the point of view of cosmic ray physics, the advantage of a Cherenkov array is that it can reconstruct depth of shower maximum at energies lower than those accessible to fluorescence telescopes.

- non-imaging detector
- Imaging Atmospheric Cherenkov Telescope (IACT)

The phenomenology of atmospheric Cherenkov emission is largely determined by how the emission angle and energy threshold depend on the index of refraction as a function of altitude. It is convenient to express the threshold of particle energy E for Cherenkov light emission in terms of the Lorentz γ-factor

$$\gamma \geqslant \frac{n(h)}{\sqrt{n(h)^2 - 1}}, \tag{16.33}$$

with $E = \gamma m$ and m the particle mass. The altitude dependence of the refractive index $n(h)$ is a function of the local air density and satisfies approximately

$$n(h) = 1 - 0.000283 \frac{\rho_{\text{air}}(h)}{\rho_{\text{air}}(0)}, \tag{16.34}$$

where ρ_{air} is the density of air. The energy threshold for electrons and the Cherenkov angle θ_{Ch} in air, $\cos\theta_{\text{Ch}} = 1/(\beta n(h))$, are given in Table A.2 as a function of altitude. Typical values at $h = 10\,\text{km}$ are $\theta_{\text{Ch}} = 0.8°$ (12 mrad) and a threshold of $\gamma = 72$, corresponding to $E = 37\,\text{MeV}$ for electrons and $E = 7.6\,\text{GeV}$ for muons.

The Cherenkov light cone of a particle at 10 km height has a radius of about 120 m at ground. This means that most of the light is expected within a circle of this radius. Due to multiple Coulomb scattering the shower particles do not move parallel to the shower axis. The angular distribution follows in first approximation an exponential

$$\frac{\mathrm{d}N_\gamma}{\mathrm{d}\theta} = \frac{1}{\theta_0} e^{-\theta/\theta_0}, \qquad \theta_0 = 0.83 \left(\frac{E_{\mathrm{th}}}{\mathrm{MeV}}\right)^{-0.67}, \tag{16.35}$$

with E_{th} being the Cherenkov energy threshold [527, 532]. Typical values of θ_0 are in the range $4 \ldots 6°$. The interplay of the altitude-dependent Cherenkov angle and the emission height leads to a characteristic lateral distribution of photons at the ground, as illustrated in Figure 16.7. The absorption and scattering of Cherenkov light in the atmosphere limits the detectable wavelength range to about $300 - 450$ nm, where the upper limit follows from the λ^{-2} suppression of large wavelengths. One possible parametrization of the lateral distribution of the Cherenkov light has the form [574]

in addition to particles at ground (electrons, muons, hadrons) in air showers electromagnetic radiation is produced:

- **Cherenkov radiation**

  charged particles moving with a speed $v > v_{air} = \frac{c}{n_{air}}$

  emitt Cherenkov radiation

  air close to ground $n \approx 1.000283 \quad \cos\Theta_c = \frac{c}{n \cdot v} \approx \frac{1}{n}$

  $\Rightarrow \Theta_c < 1.4^\circ$ **in air**

  Cherenkov threshold $E_e = 22\ \mathrm{MeV} \quad E_\mu = 4.4\ \mathrm{GeV}$

  --> most Cherenkov light is emitted from relativistic electrons

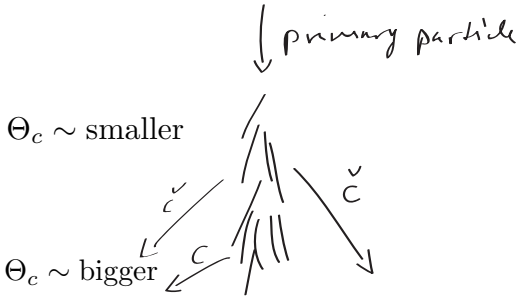

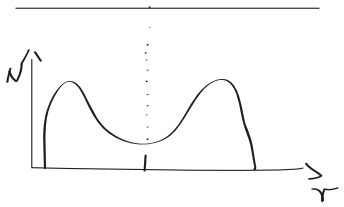

focusing effect due to increase of *n* with increasing depth --> *n(h)* $\Rightarrow \Theta_c = f(h)$

ring with ~100 m diameter on the ground

e.g. 1 TeV gamma ray produces ~3*10^6 Cherenkov photons 300-500 nm

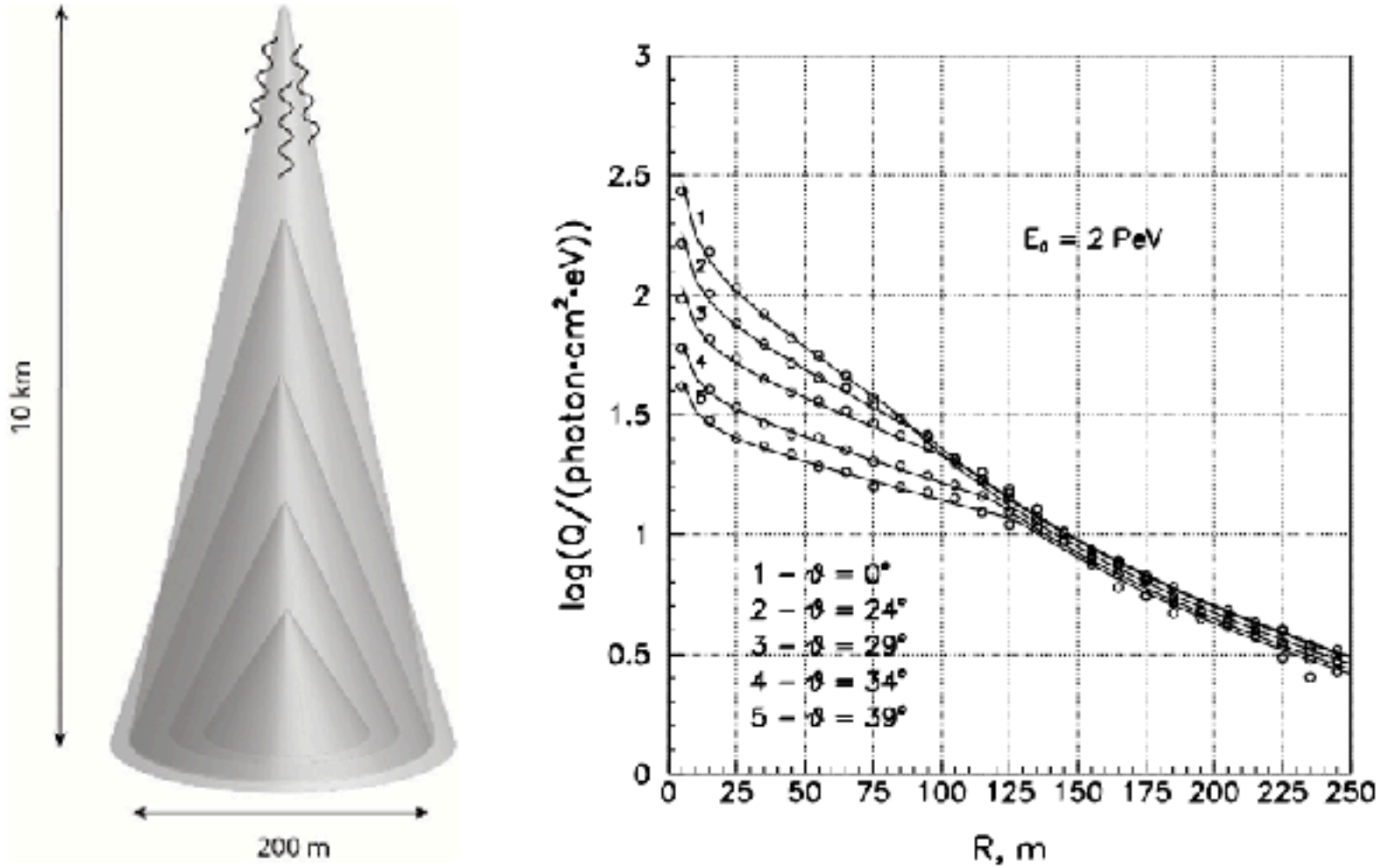

Figure 16.7 **Left:** Illustration of the relation between production height and Cherenkov opening angle for producing the observed Cherenkov light distribution at ground. **Right:** Simulated lateral distributions of Cherenkov light produced by proton-induced showers of different zenith angle [572]. The simulations were done for a height of 2000 m above sea level.

One possible parametrization of the lateral distribution of the Cherenkov light has the form [574]

$$C(r) = \begin{cases} C_{120} \cdot \exp(a[120\,\mathrm{m} - r]); & 30\,\mathrm{m} < r \leqslant 120\,\mathrm{m} \\ C_{120} \cdot (r/120\,\mathrm{m})^{\ b}; & 120\,\mathrm{m} < r \leqslant 350\,\mathrm{m} \end{cases}, \tag{16.36}$$

with the parameters C_{120}, a and b.

Clear, moonless nights are required for taking data with air Cherenkov detectors, resulting in an effective duty cycle of $10 - 15\%$. Also continuous monitoring of the atmospheric conditions including the density profile of the atmosphere is necessary [575].

Arrays of photodetectors are used in non-imaging Cherenkov experiments to sample the lateral distribution of light in dark and clear nights. After reconstructing the core position, the measured parameter C_{120} and the slope are linked to the properties of the primary particle. Simulations show that the density of photons at 120 m from the core is almost directly proportional to the energy of the shower and that the slope is related to the depth of shower maximum [573]. Examples of surface arrays applying this non-imaging technique of shower detection via Cherenkov light are AIROBICC [576], EAS-TOP [577], BLANCA [574], Tunka [568] and Yakutsk [569]. The latter two are currently in operation, with Tunka being extended from an array of originally 25 stations to 133.

Measurement of Čerenkov light

two techniques

1) non-imaging detectors open Č detectors

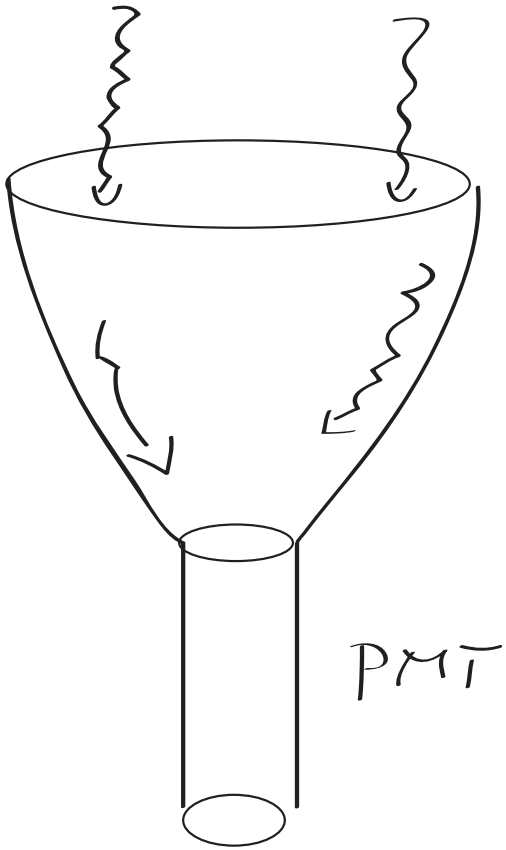

$\phi \sim 0{,}5\,\mathrm{m}$

Winston cone to collect light

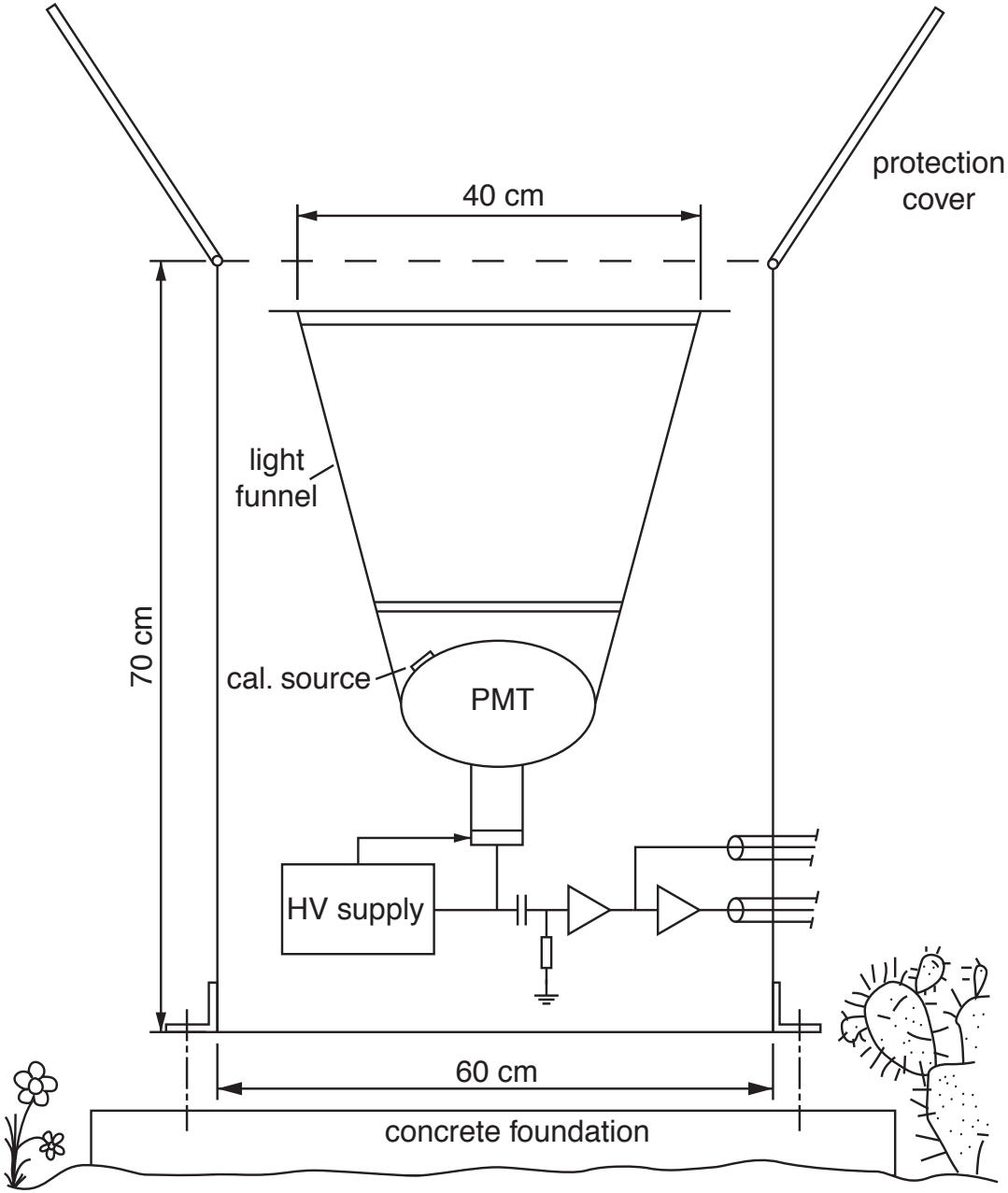

Fig. 4.19. Integrating Cherenkov cone of an AIRO-BICC station and auxiliaries. Directly above the PMT a glass filter restricted the incoming light to wavelengths smaller than 500 nm and a plexiglass cover protected against dew, white frost and dust [29]

Single event in CASA-BLANCA

CASA

measures particles,
determines shower core

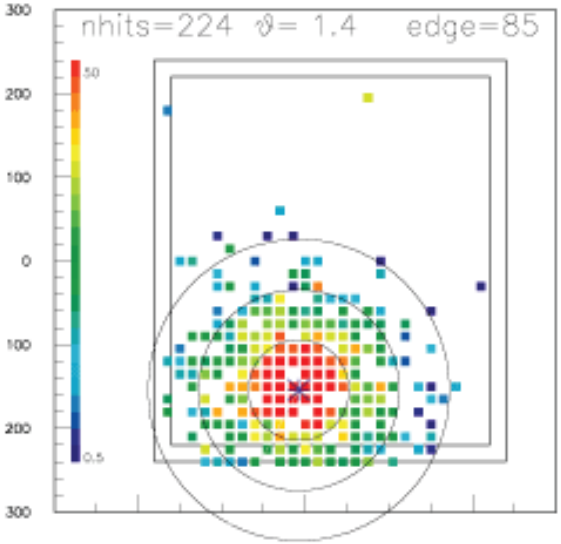

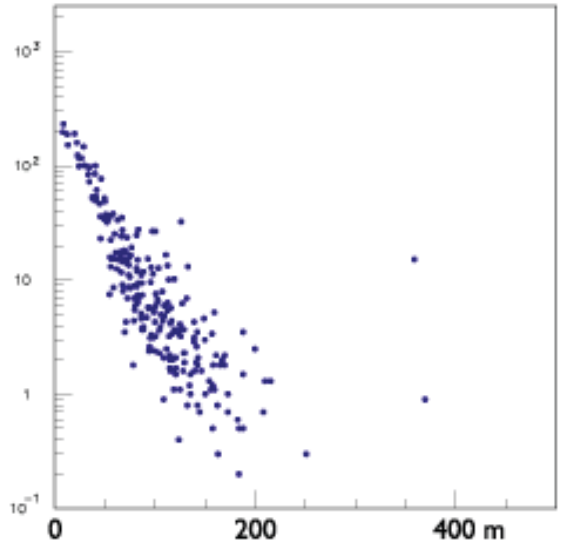

BLANCA

measures Cherenkov light,
determines lateral C-distribution

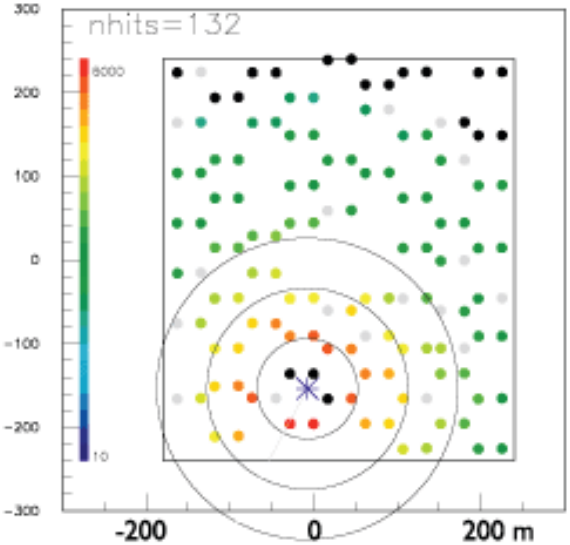

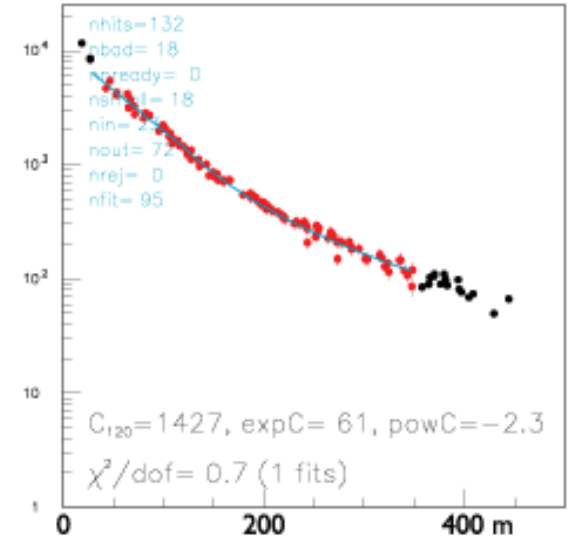

Tunka Experiment

Lateral distribution of Cerenkov light

$$C(r) = \begin{cases} C_{120} \times \exp(s[120\,\mathrm{m} - r]) & 30\ \mathrm{m} < r < 120\ \mathrm{m} \\ C_{120} \times (r/120\,\mathrm{m})^{-\hat{a}} & 120\ \mathrm{m} < r < 350\ \mathrm{m} \end{cases}$$

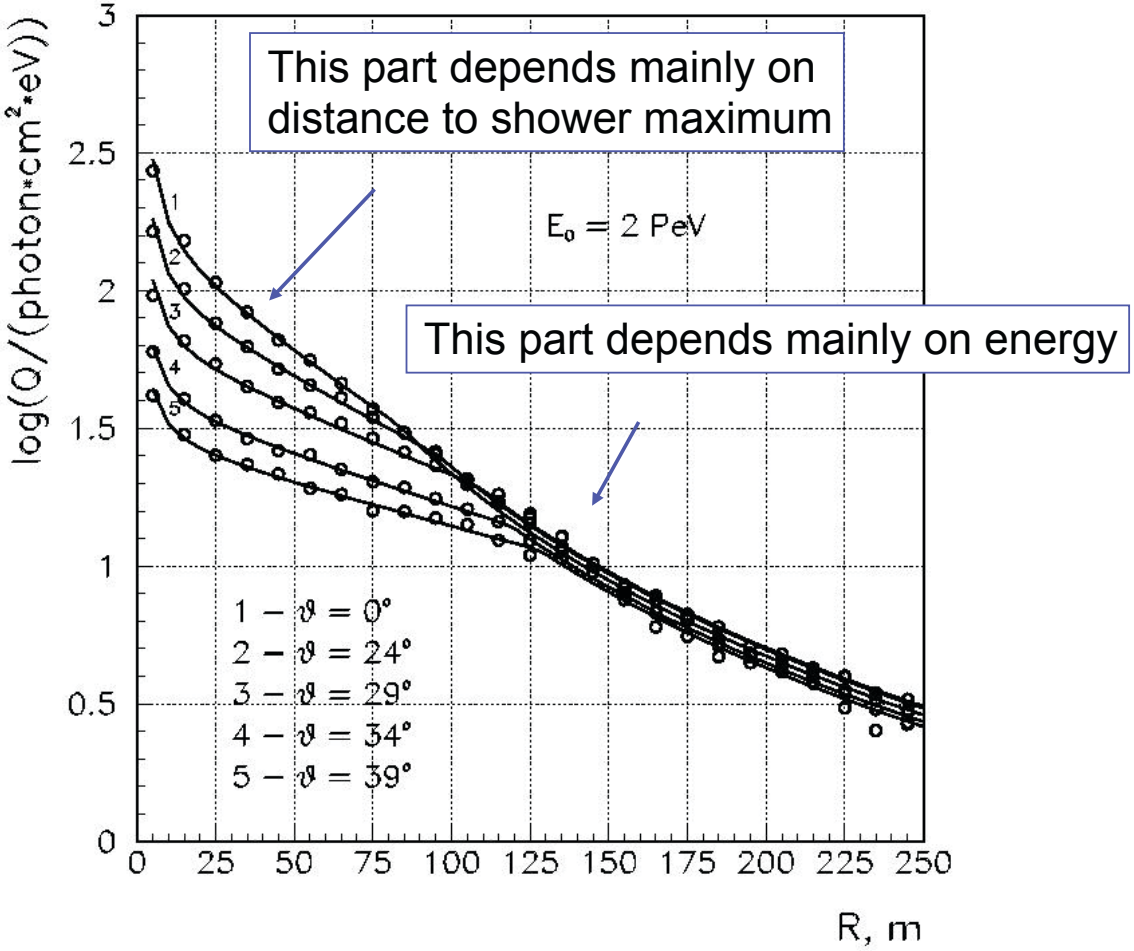

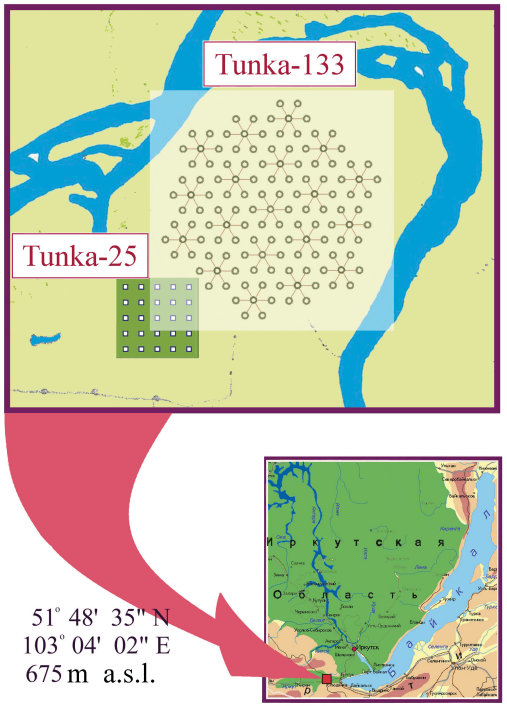

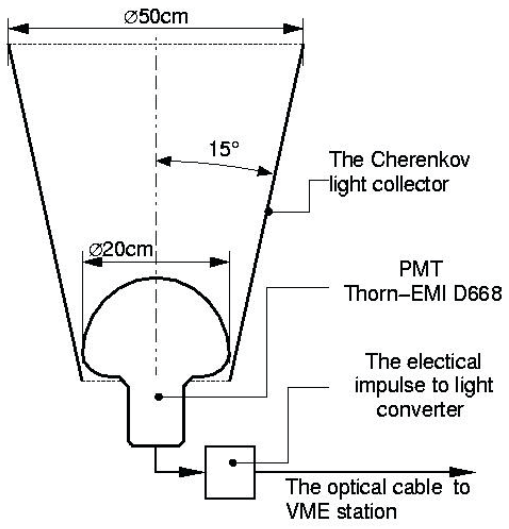

Ch. Spiering, DPG 2005

Imaging Atmospheric Cherenkov Telescope (IACT)

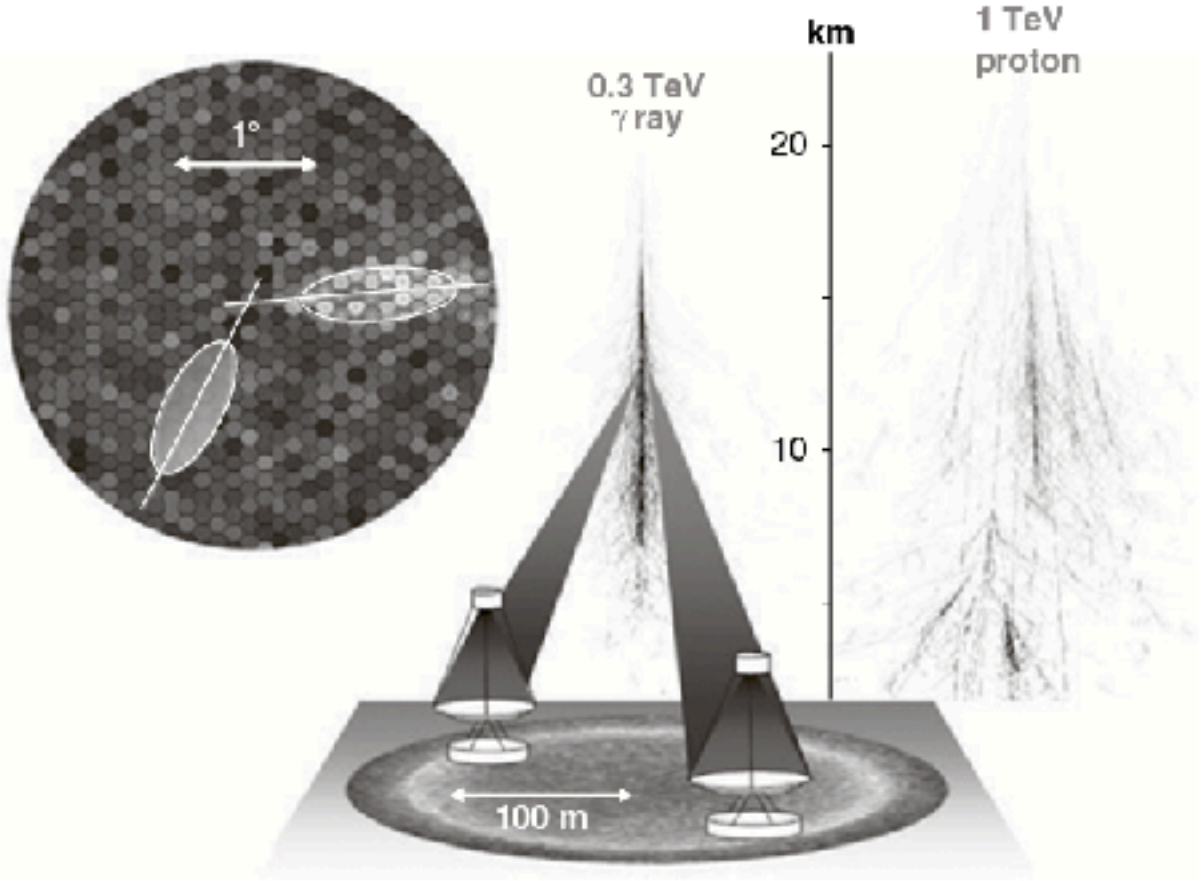

Figure 16.8 Illustration of the stereo-detection principle of imaging atmospheric Cherenkov telescopes [567]. The superimposed camera images are shown on the left-hand side. The intersection of the shower axes in this combined image corresponds to the arrival direction of the shower. From [567], © 2009 by Annual Reviews (www.annualreviews.org), reproduced with permission.

H.E.S.S. telescope, Namibia

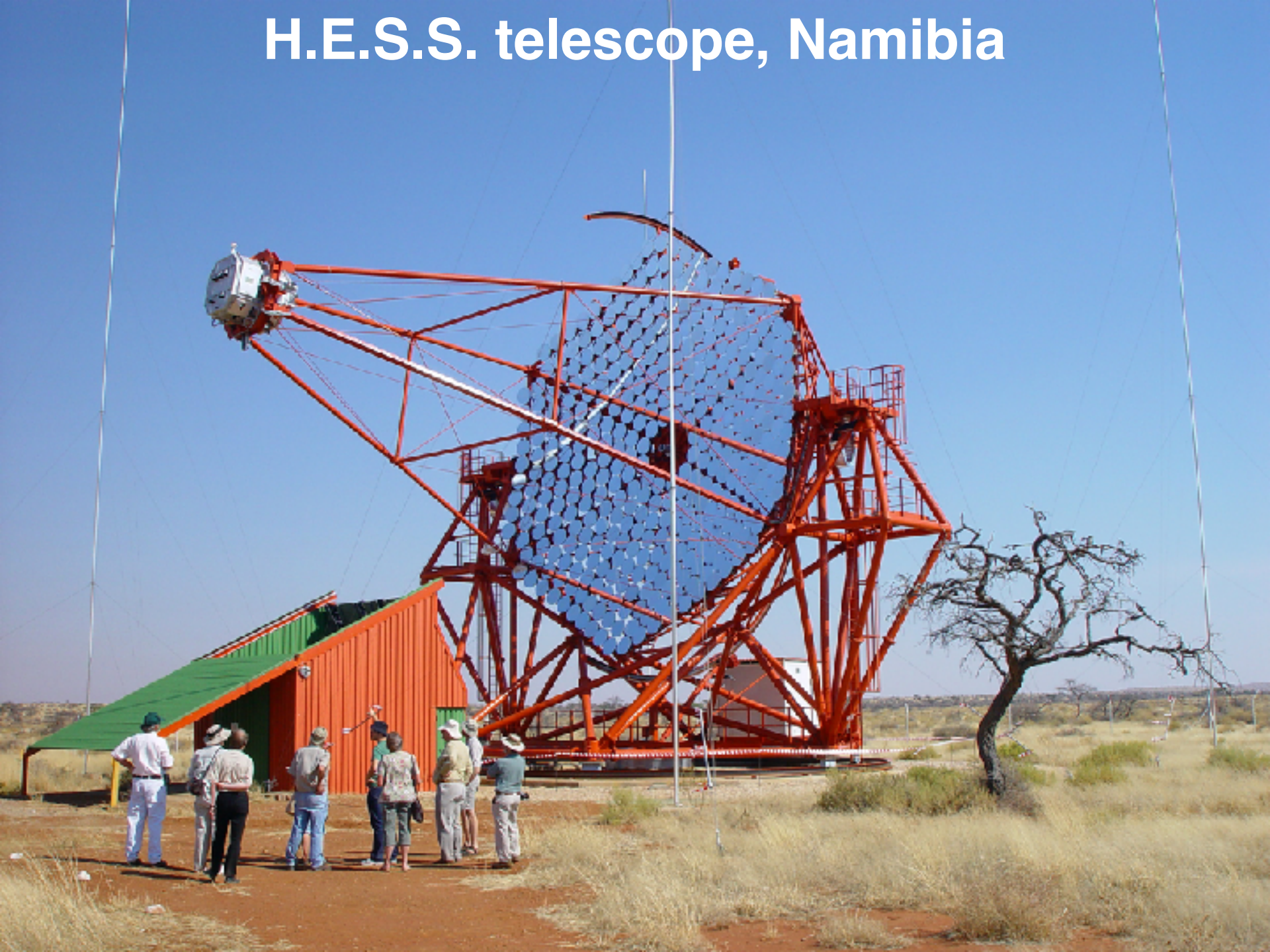

H.E.S.S. telescope, Namibia

H.E.S.S. telescope, Namibia

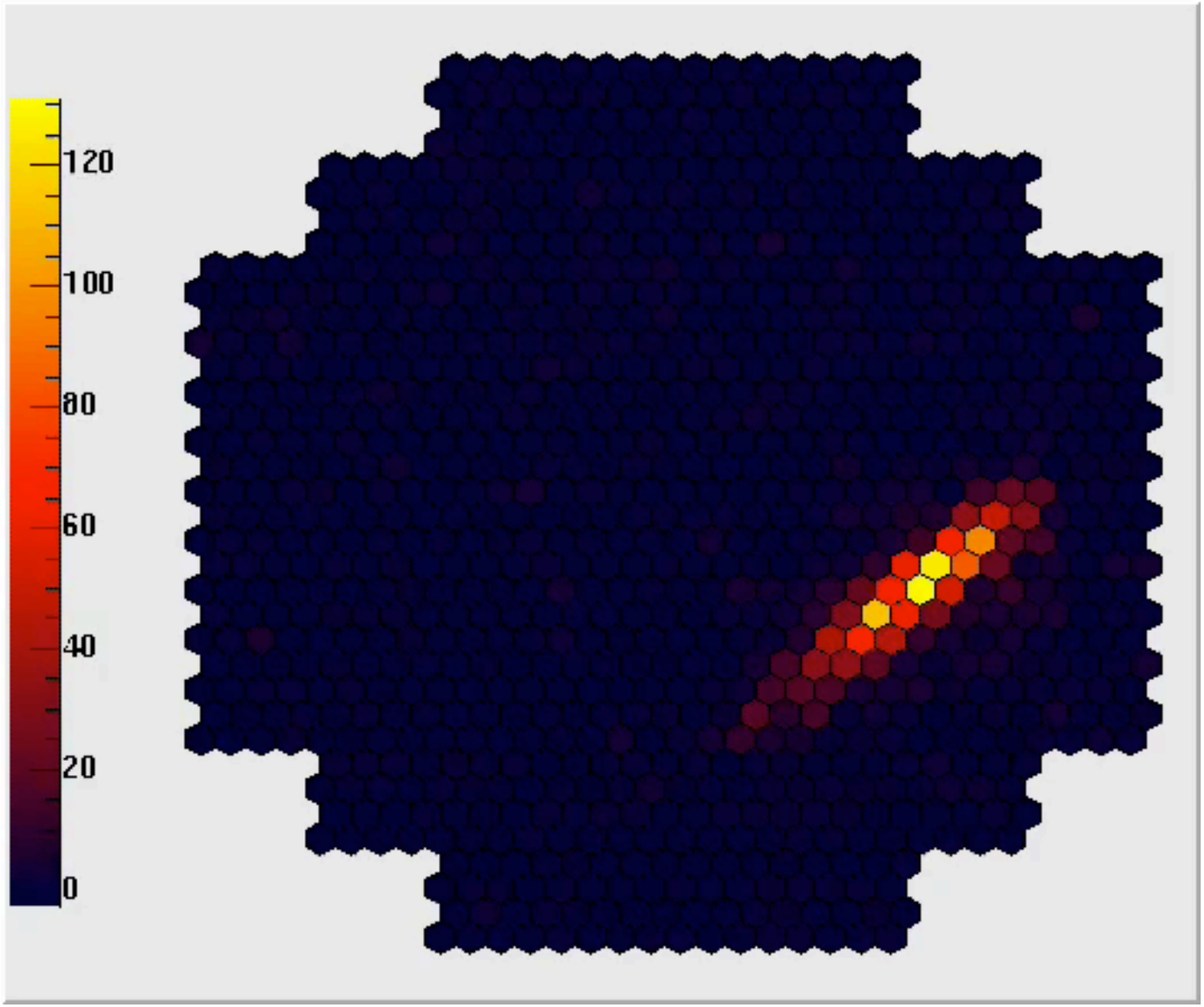

- **Fluorescence light**

charged particles moving through the atmosphere excite nitrogen molecules

--> fluorescence light (300-450 nm)

isotropic radiation of fluorescence light

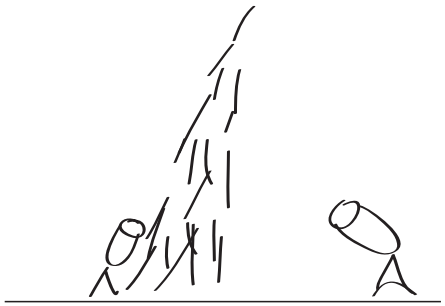

--> air showers can be observed from aside

~0.5% of dE/dx (~2.2 MeV/(g cm²)

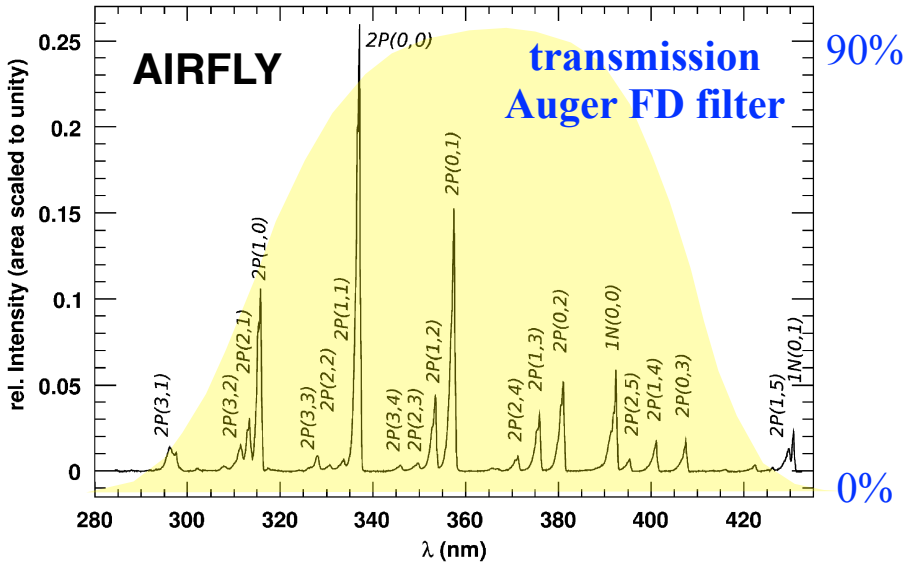

Fig. 2. Air-fluorescence spectrum excited by 3 MeV electrons at 800 hPa as measured by the AIRFLY Collaboration [32].

Hybrid Detector

Fluorescence light telescope

Surface array
(water Cherenkov detectors)

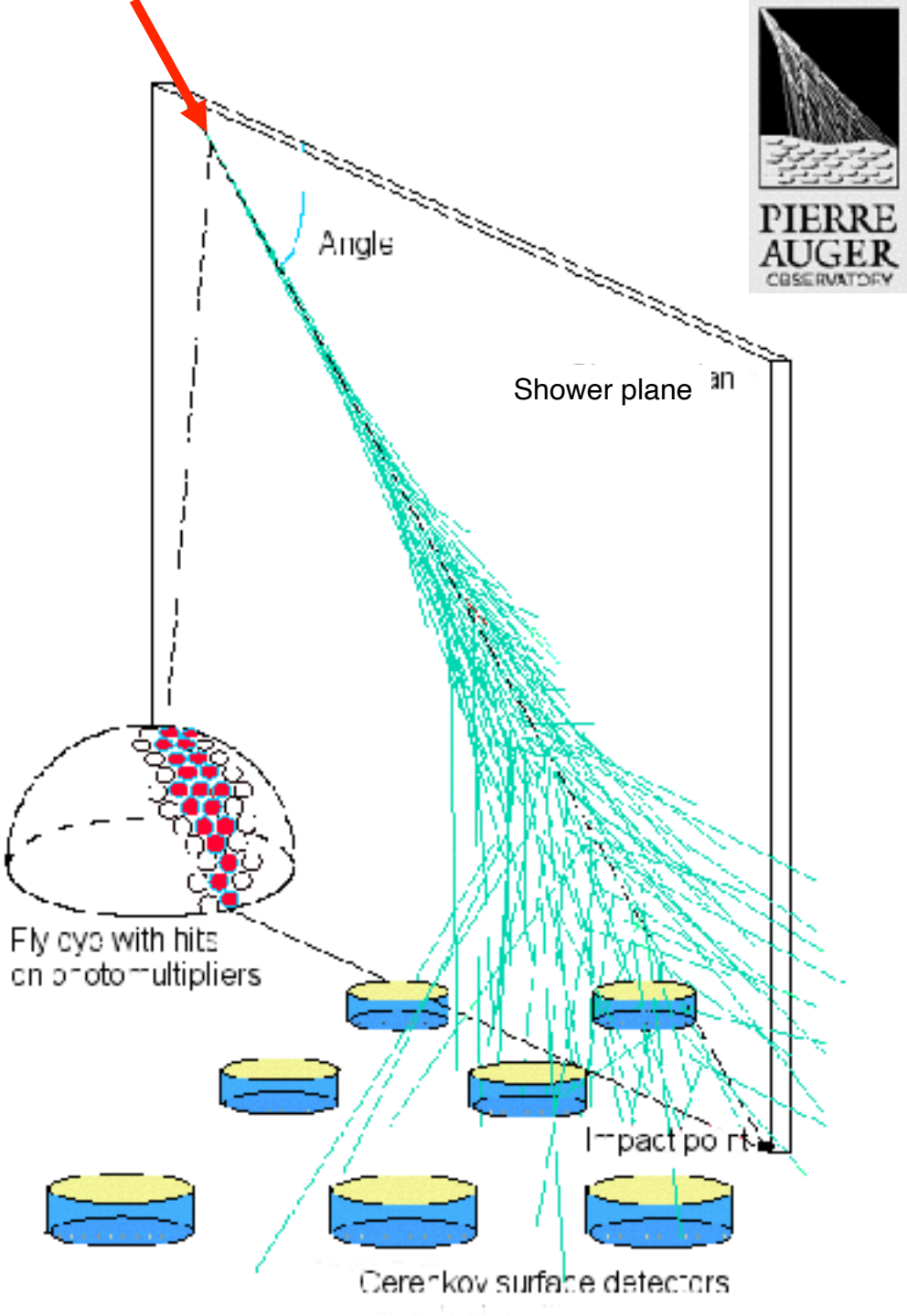

FD eye view

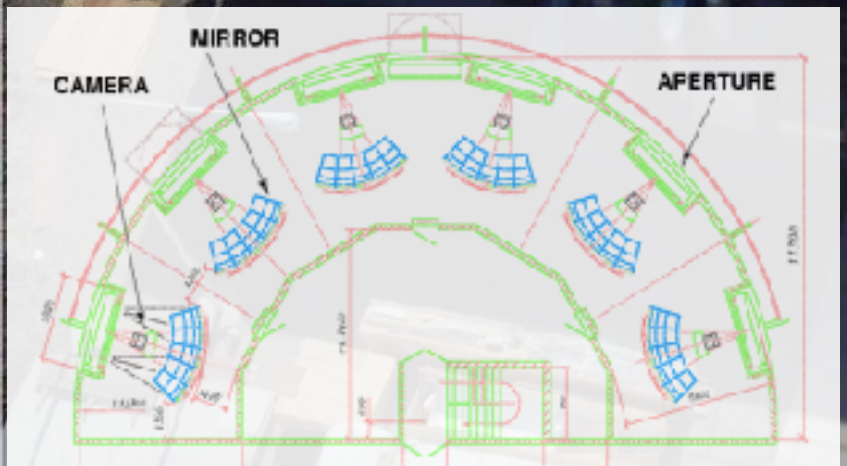

Four sites
Six telescopes
viewing 30°x30° each

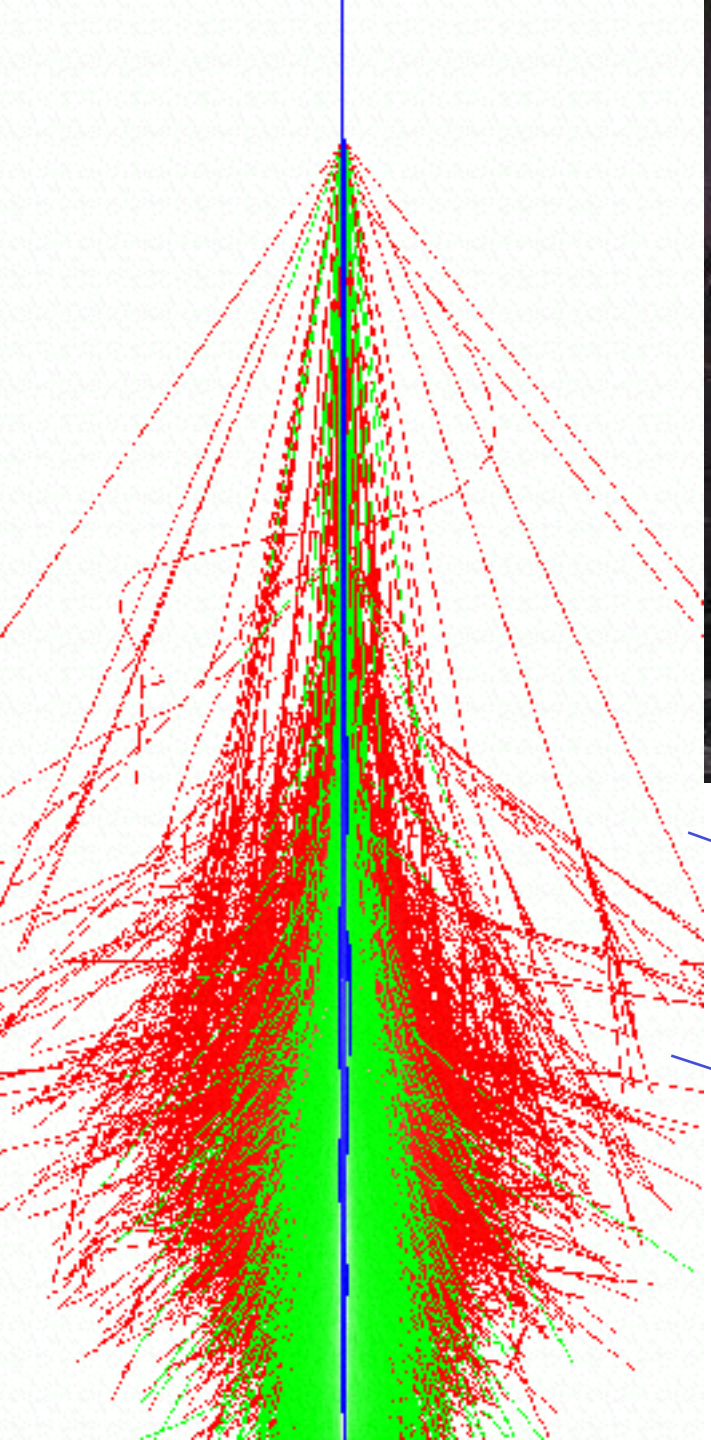

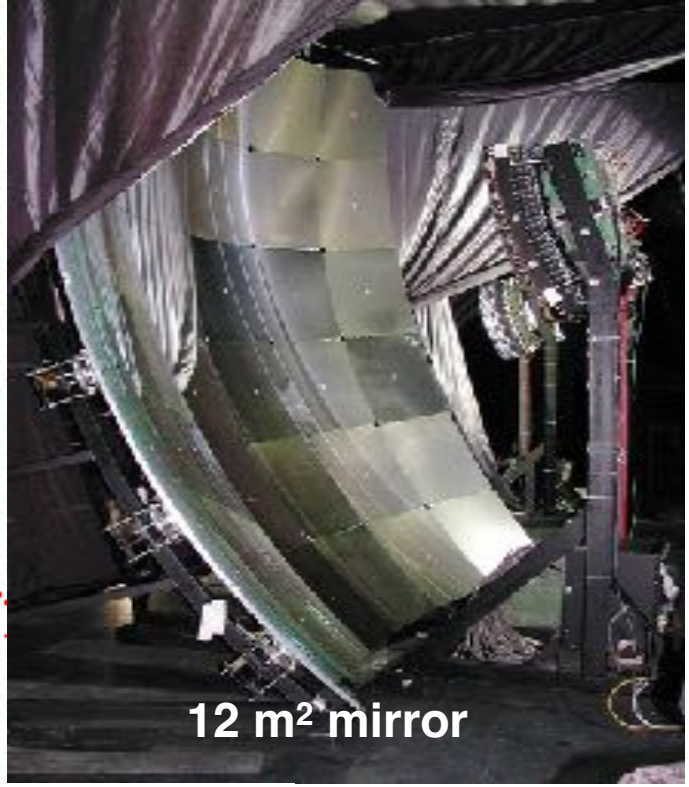
12 m² mirror

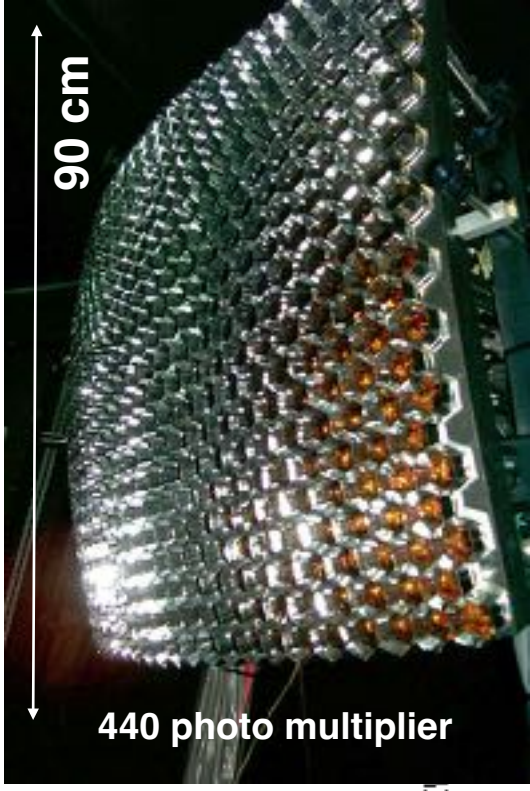
90 cm
440 photo multiplier

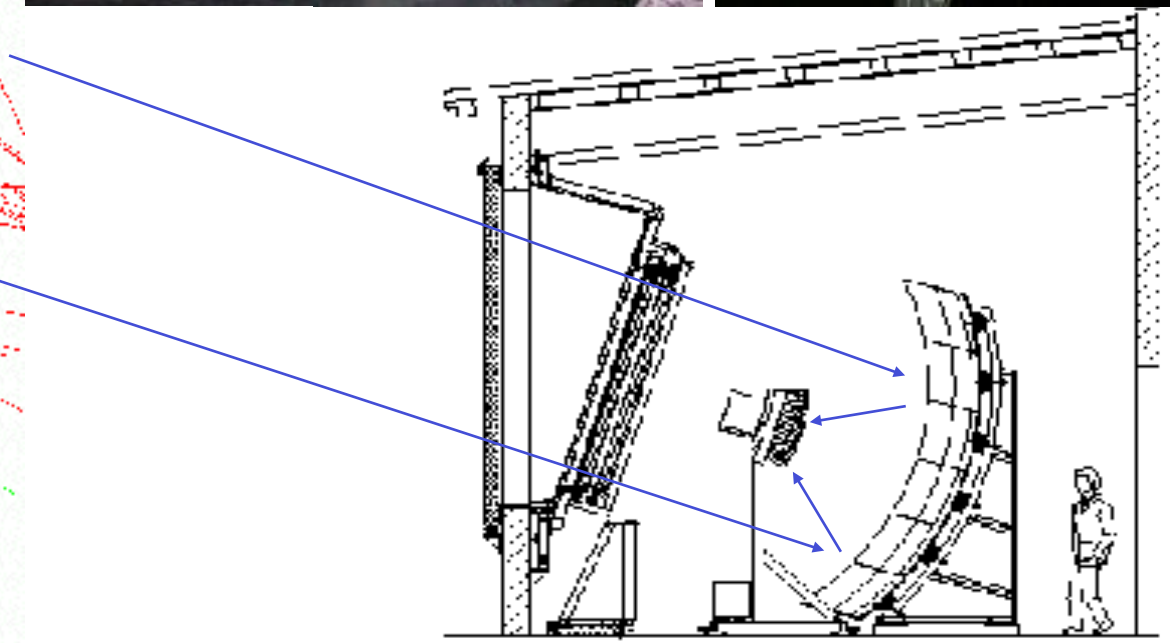

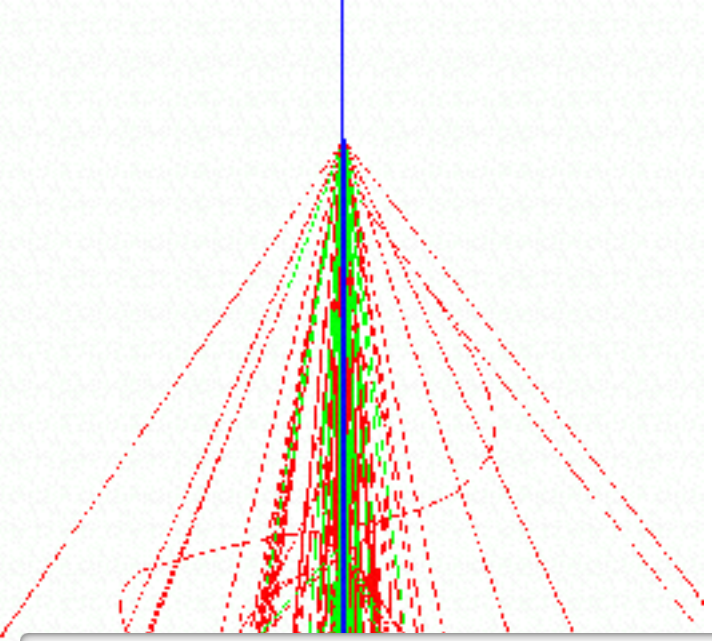

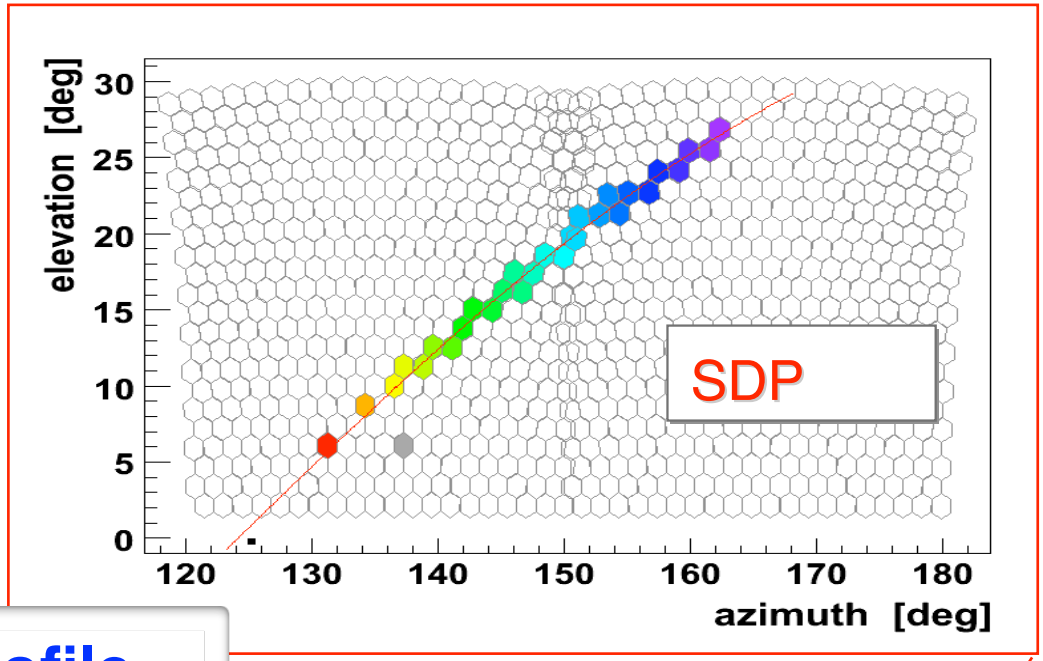

longitudinal shower profile

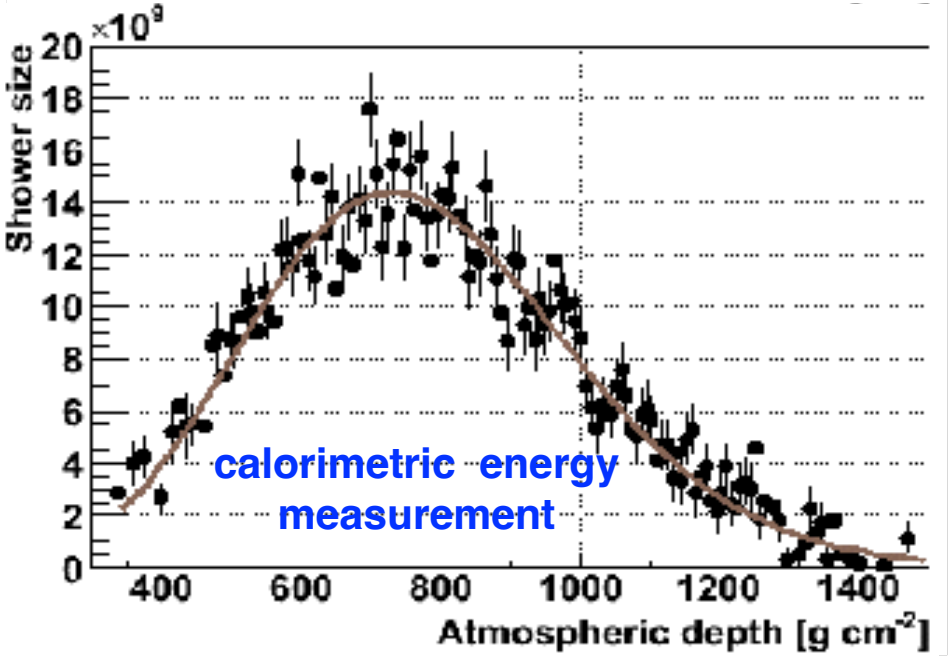

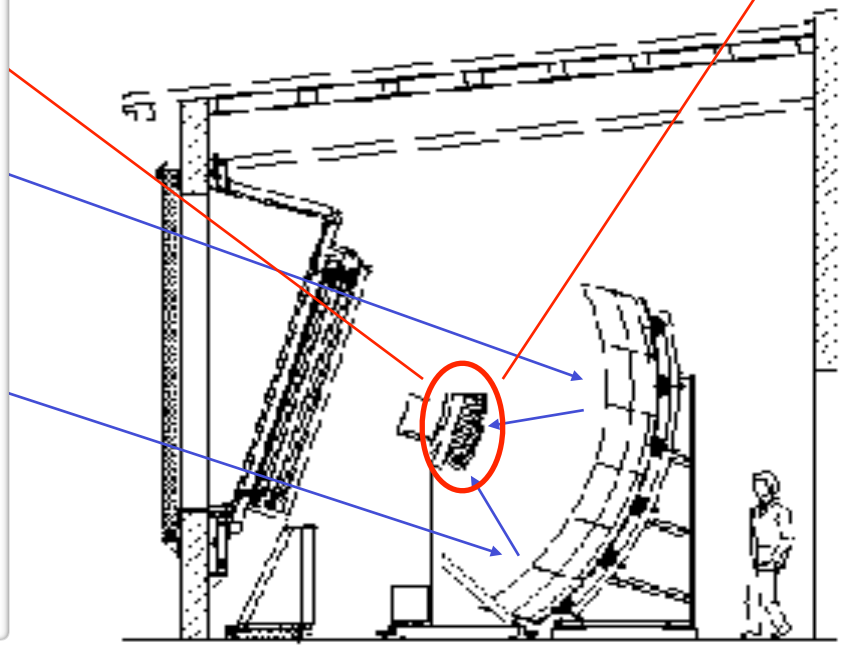

The function proposed by Gaisser and Hillas [598] gives a good phenomenological description of individual as well as averaged longitudinal shower profiles

$$N(X) = N_{\max} \left(\frac{X - X_1}{X_{\max} - X_1} \right)^{(X_{\max} - X_1)/\Lambda} \exp\left(- \frac{X - X_{\max}}{\Lambda} \right). \quad (16.38)$$

It is often used to extrapolate the measured shower profiles to depth ranges outside the field of view of the telescopes and to fit for $N_{\max}$ and $X_{\max}$. In doing so, X_1 and $\Lambda = 55 - 65\,\mathrm{g/cm^2}$ are parameters of the fit. In particular, X_1 can be negative. The same function with $X_1 > 0$ interpreted as the point of first interaction is sometimes used as a toy model to illustrate fluctuations in air shower, as discussed in Appendix A.8.

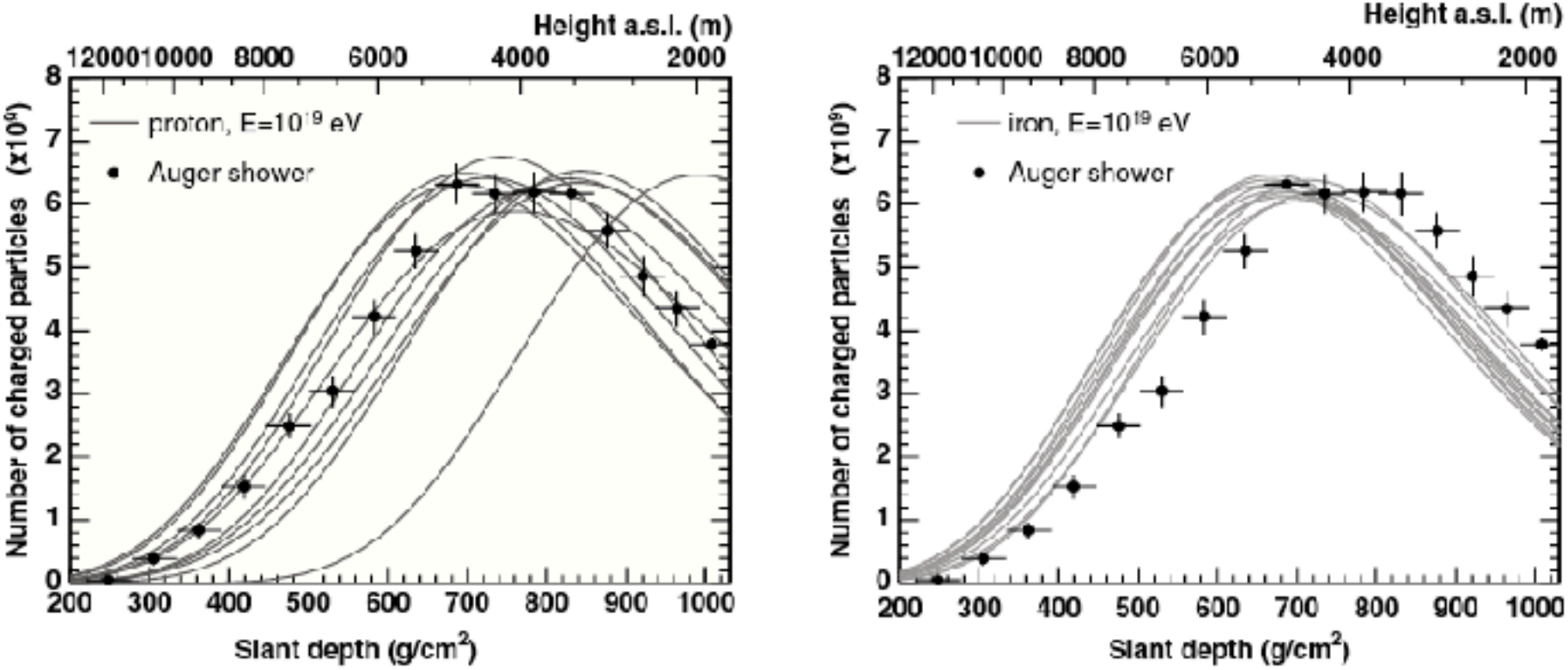

Figure 16.9 Profile of one shower measured with the Pierre Auger Observatory [594]. The reconstructed energy of this shower is about 10^{19} eV. The data are shown together with 10 simulated proton (left) and 10 iron showers (right) to demonstrate the composition sensitivity of the depth of shower maximum. The showers were simulated with the Sibyll interaction model [158, 520] and the CONEX air shower package [514].

A Hybrid Event

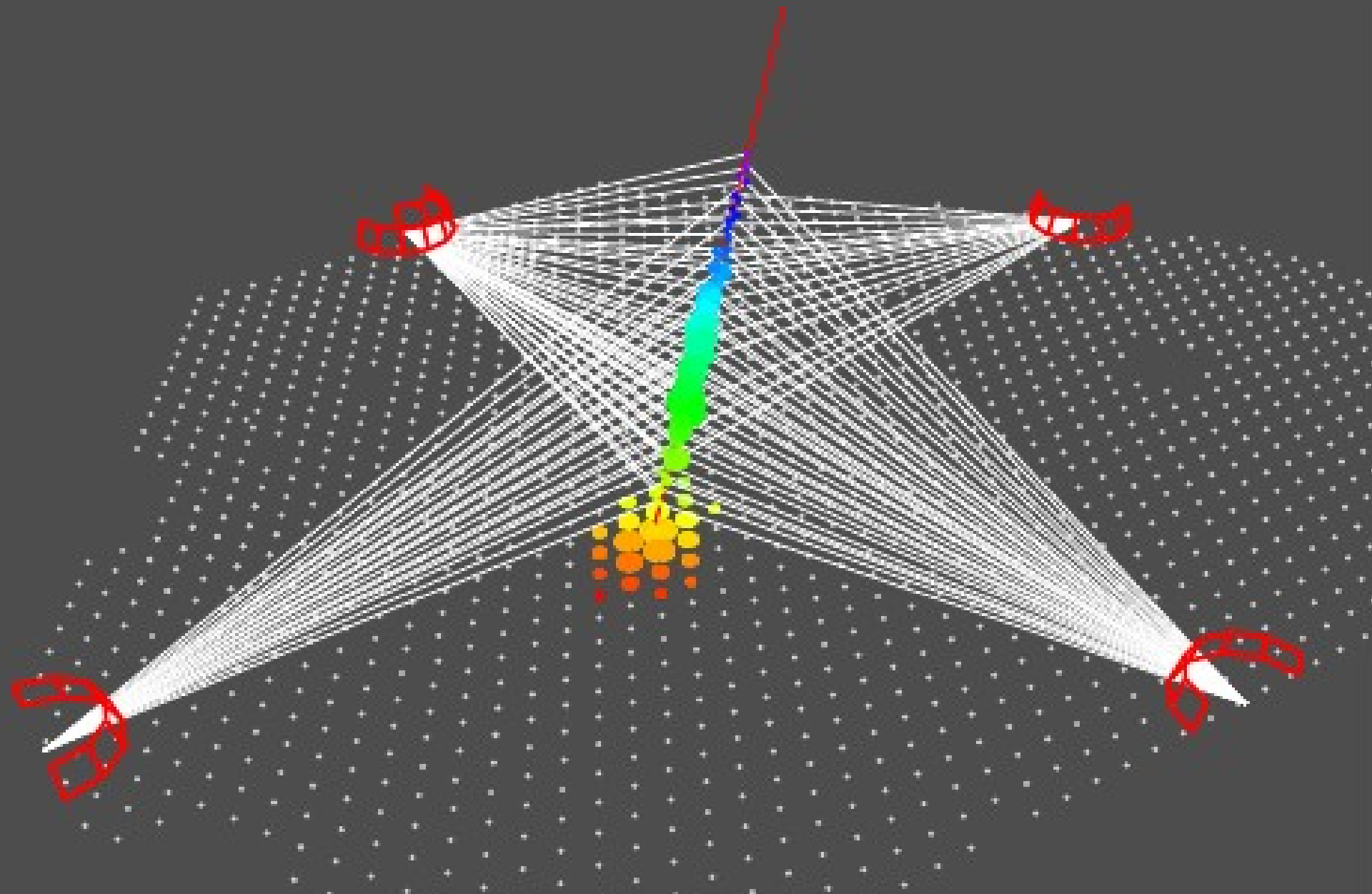

Telescope Array Observatory

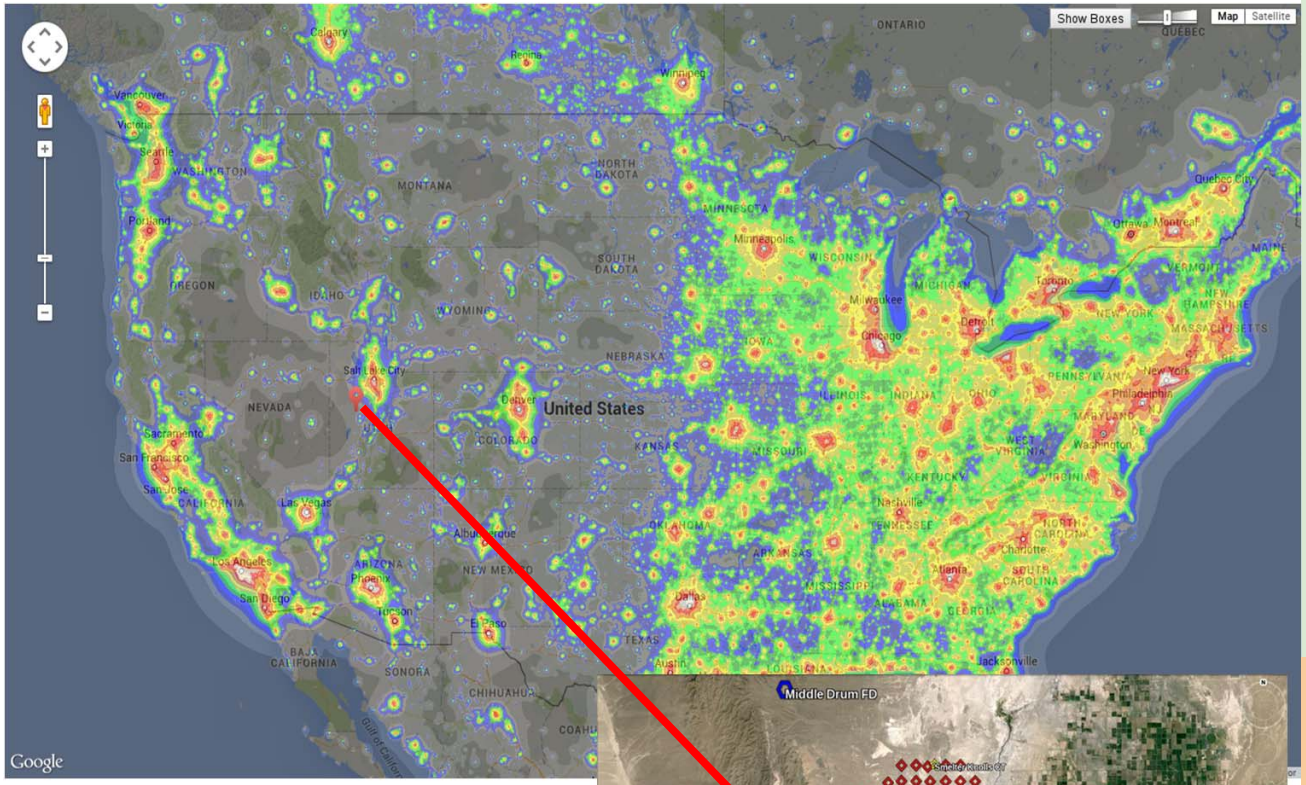

U.S. Light Pollution Map

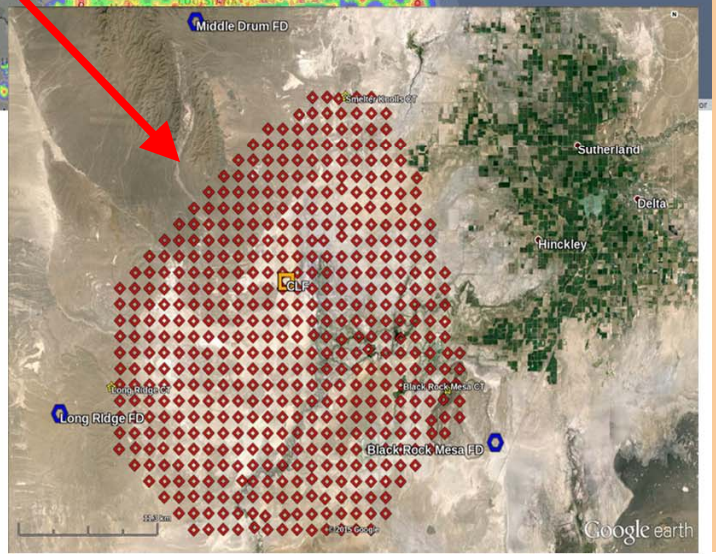

Largest cosmic ray observatory in the Northern hemisphere.

~700 km^2 → ≲ *land* area of New York City.

Millard County, Utah
39.30° N
112.91° W
1550 m ASL

~800 g/cm^2 vertical depth

The High Energy component of Telescope Array – 38 fluorescence telescopes (9728 PMTs) at 3 telescope stations overlooking an array of 507 scintillator surface detectors (SD) - operational as of 2008.

TA Fluorescence Detectors

Middle Drum

14 telescopes @ station
256 PMTs/camera

5.2 m^2

Reutilized from HiRes-I

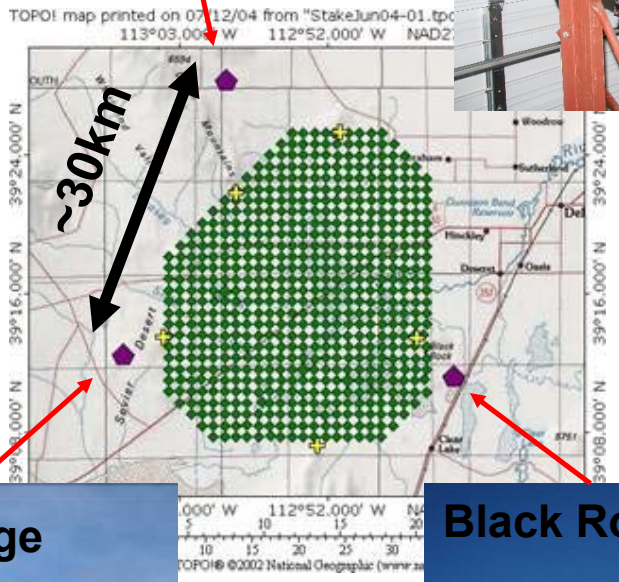

New Telescopes

12 telescopes/station
256 PMTs/camera

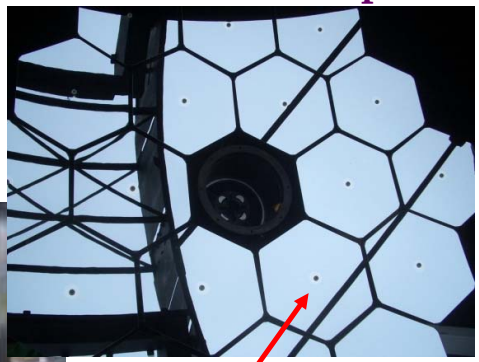

6.8 m^2

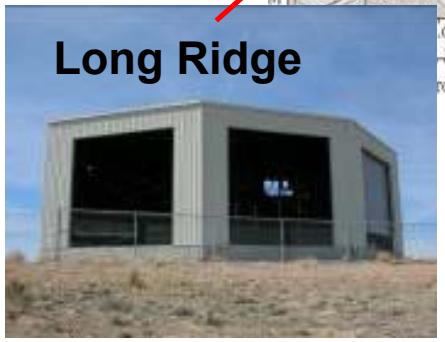

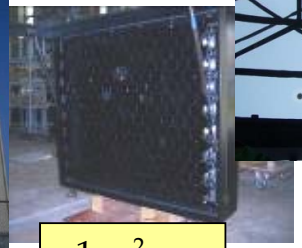

~1 m^2

Typical Fluorescence Event

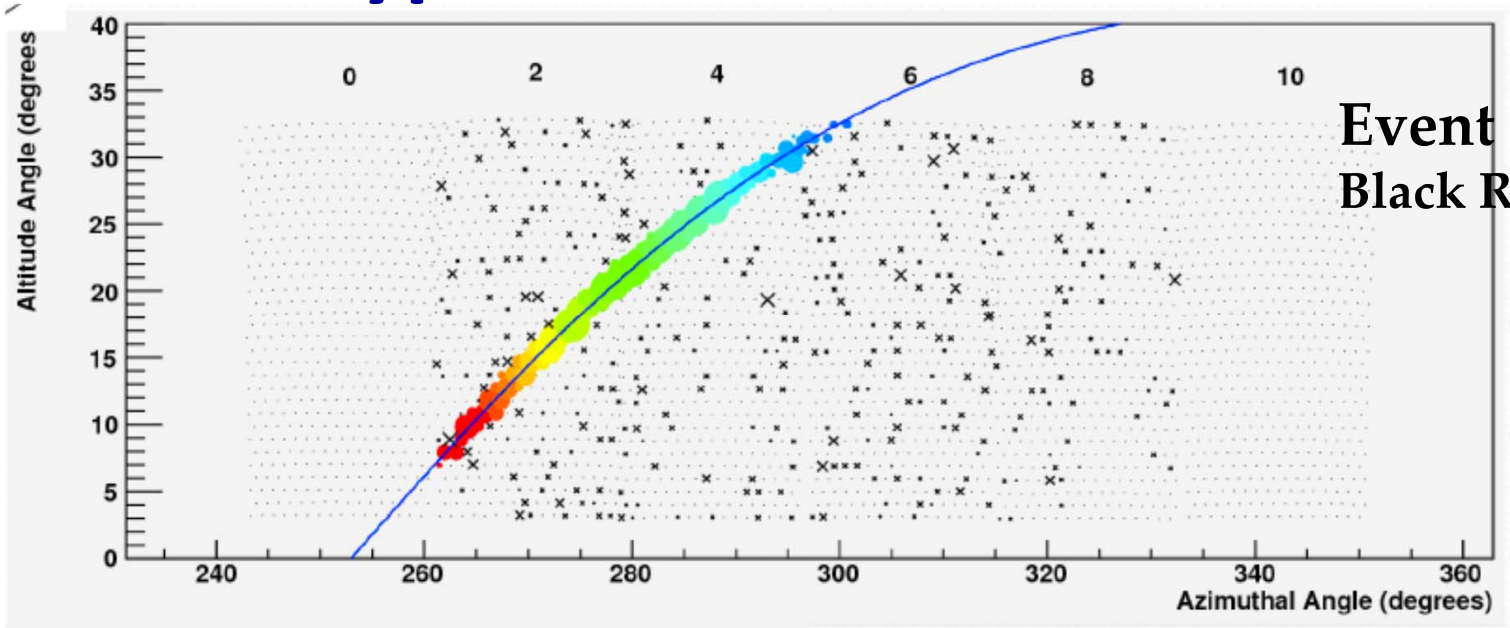

Event Display
Black Rock Mesa

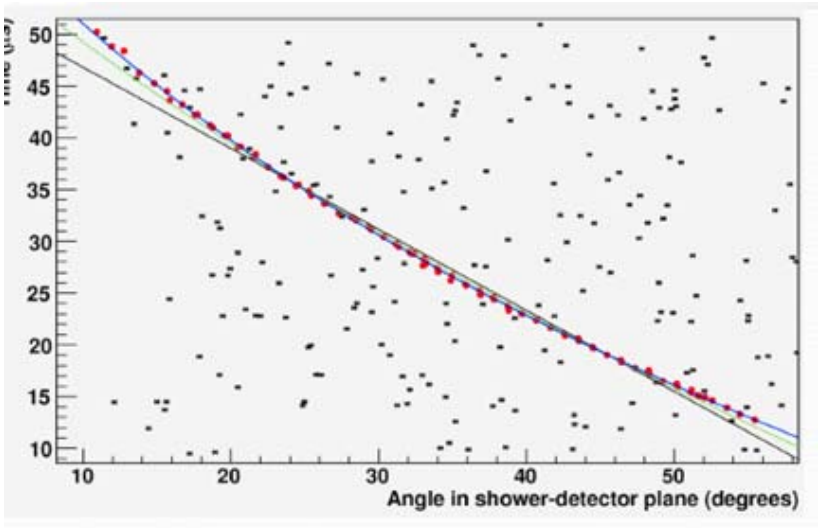

Monocular timing fit (time vs angle)

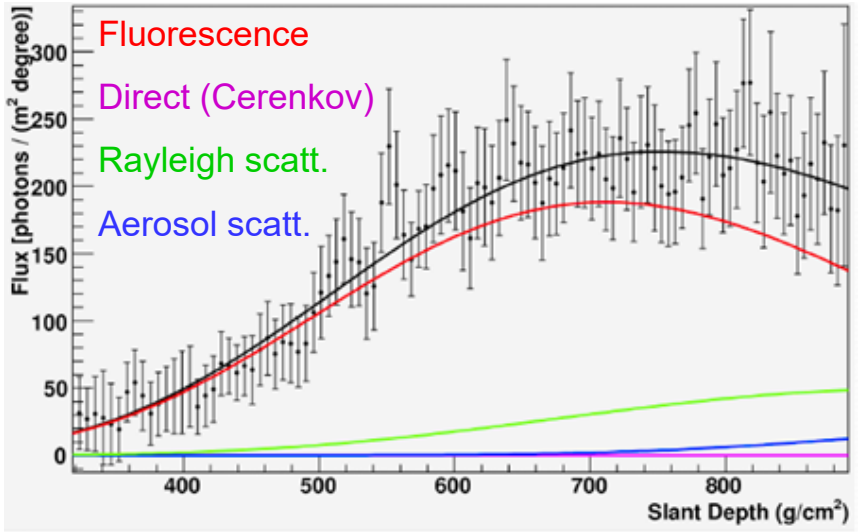

Reconstructed Shower Profile

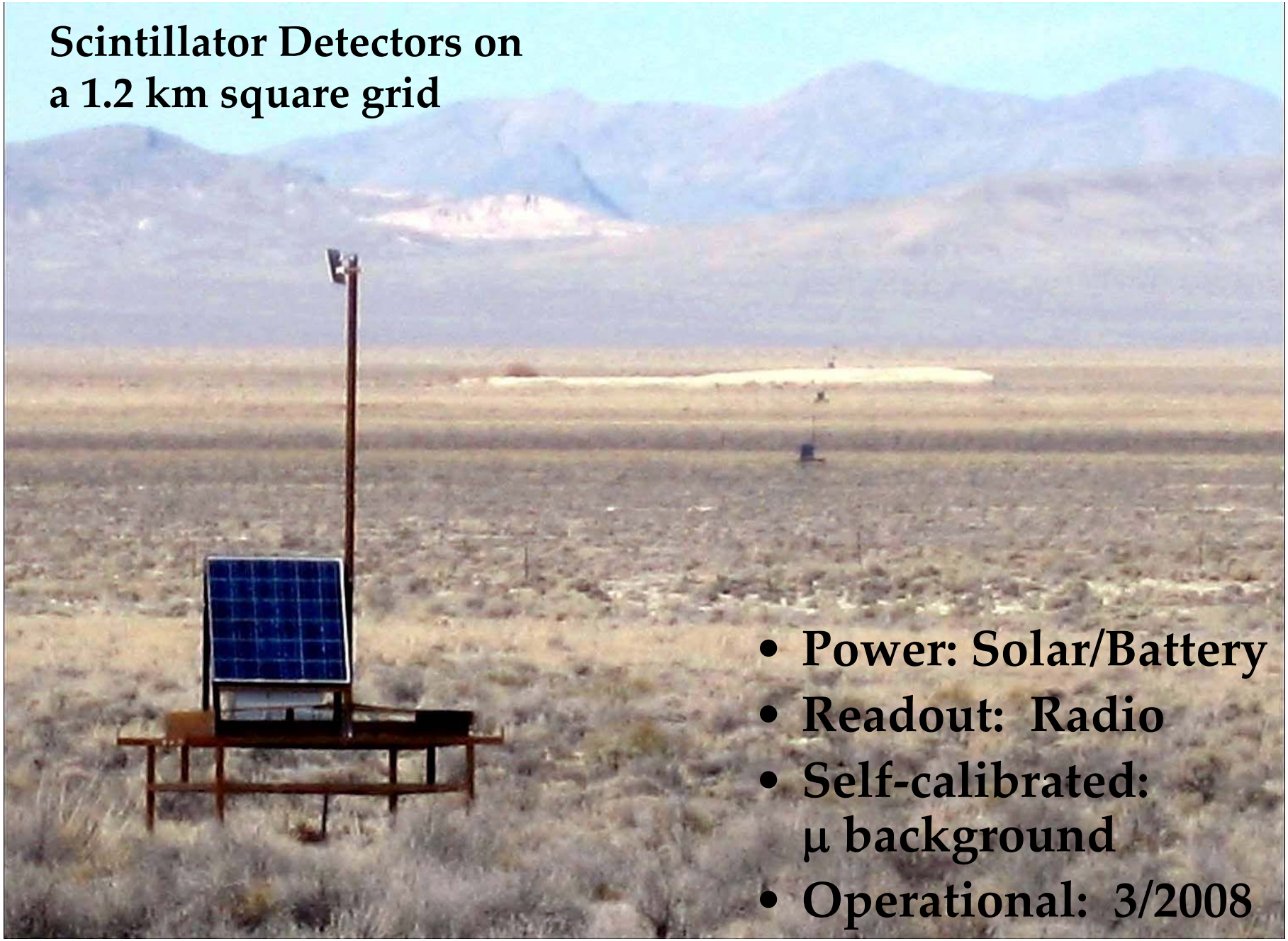
Scintillator Detectors on
a 1.2 km square grid
• Power: Solar/Battery
• Readout: Radio
• Self-calibrated:
μ background
• Operational: 3/2008

Example Event

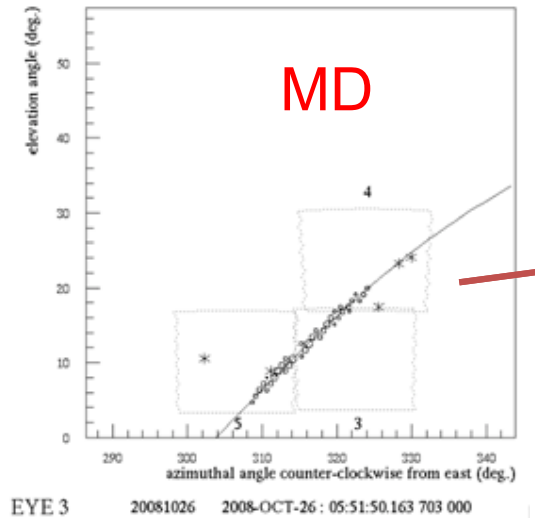

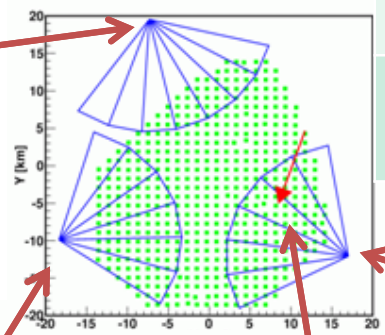

	θ [°]	ϕ [°]	x[km]	y[km]
MD mono	51.43	73.76	7.83	-3.10
BR mono	51.50	77.09	7.67	-4.14
Stereo BR&LR	50.21	71.30	8.55	-4.88

Event from 2008-10-26